Functional characterization of ErbB3-binding protein 1 (EBP1) tumor mutants

Elisabeth Johnsen Lind

This thesis is submitted in partial fulfilment of the requirements for the degree of Master of Science at:

Department of Biological Science,

Faculty of Mathematics and Natural Sciences,

University of Bergen, Norway,

June 2021.

Acknowledgements

The work presented in this thesis was conducted from August 2020 to June 2021 at Department of Biological Science, Faculty of Mathematics and Natural Sciences, University of Bergen, Norway.

First, I would like to thank my supervisor associate professor Aurélia E. Lewis for all the help with my thesis, consistently motivating, kind and pushing me forward. Your understanding and knowledge of the field is impressive and your passion contagious. You have used this quality to help me with planning, executing, and interpreting my results as well as teaching me extensively about little and small. You have gone above and beyond to help me succeed with my thesis, in this time of the COVID-19 pandemic and always answered my questions and messages at any time.

I would also like to thank my co-supervisor Diana C. Turcu, you have been amazing, and this project could truly not have happened without you. Your participation in this project have been invaluable and you have taken part in all my experiments in one way or another, particularly with the thermal denaturation experiment. With your incredible patience you have thought me laboratory methods and techniques, shared your personal work expertise, given advice, answered questions, and helped me when I have messed up in the lab.

Thank you to Andrea P. Morovicz, who also was my co-supervisor. It has been so much fun working on the EBP1 project with you. You have been so kind, knowledgeable and helpful, advising me on how best to work with EBP1 and cell cultures.

In addition, I would like to thank Sandra Ninzima, for all the help you have given, especially with cell work and using instruments, as well as troubleshooting. I would also like to say thank you to Andreas Midlang, you have been my fellow master student and office mate. I have really enjoyed sharing an office with you, discussing our projects and learning from your many good ideas.

I also want to thank the entire NucReg group, the people at Mol-Bio and my fellow master students for creating an amazing work environment, with friendly smiles, helpful attitudes, ready to troubleshoot and inject good ideas when things did not work as I would wish. Even though we have been going through a pandemic, with all its big and small challenges, you have all together made working on the thesis a great experience.

Lastly, I would like to thank my family, particularly mom, dad and brother Andreas for supporting me through my studies. Thank you mom for always looking after my wellbeing, your kind heart and wisdom. Thank you, dad and Andreas, for helping me set up and perfecting my home office, and giving me understanding, compassion and invaluable academic advice.

Innhold

Selected abbreviations

Akt	Protein kinase B
CDK	Cyclin dependent kinase
CHIP	Carboxy terminus of HSP70-interacting protein
DAG	Diacylglycerol
DFC	Dense fibrillar component
EBP1	ErbB3 binding protein 1
EGFP	Enhanced Green Fluorescent Protein
ER	Endoplasmic reticulum
FBXW7	F-box and WD40 domain protein 7
FC	Fibrillar center
FL	Full length
GC	Granular component
HRG	Heregulin
HSP70	Heat shock protein 70
IRES	internal ribosome entry site
K/R motif	Lysine/arginine rich motif
MAP	Methionine aminopeptidases
MDM2	E3 ubiquitin-protein ligase Mdm2
NC	Nucleocapsid
NLS	Nuclear localization signal
NoLS	Nucleolar localization signal
NoRS	Nucleolar retention signal
PA2G4	Proliferation associated 2 G4
PBR	Polybasic region
PH domain	Pleckstrin homology domain
PI3K	Phosphoinositide-3 Kinase
PIPK	phosphatidylinositol phosphate kinases
PKC	Protein Kinase C
PLC	Phospho Lipase C
PPIn	Polyphosphoinositide
PtdIns	Phosphatidylinositol
PtdIns(3,4,5)P_3	Phosphatidylinositol (3,4,5)-trisphosphate
PtdIns(3,4)P_2	Phosphatidylinositol (3,4)-bisphosphate

PtdIns(3,5)P_2	Phosphatidylinositol (3,5)-bisphosphate
PtdIns3P	Phosphatidylinositol 3-phosphate
PtdIns(4,5)P_2	Phosphatidylinositol (4,5)-bisphosphate
PtdIns*4P*	Phosphatidylinositol 4-phosphate
PtdIns*5P*	Phosphatidylinositol 5-phosphate
Rb	Retinoblastoma
rDNA	ribosomal DNA
rRNA	ribosomal RNA
UBF	Upstream binding factor

Abstract

ErbB3 binding protein 1 (EBP1) is an ubiquitous protein taking part in many cell processes such as, cell cycle regulation, proliferation and survival as well as interactions with DNA, RNA and other proteins. EBP1 localizes in the cytoplasm and nucleoli where riboproteins, proteins, and lipid aggregate for interactions. PPIn in the nucleus have been discovered to interact with EBP1. EBP1 is a highly conserved protein from the peptidase M24 family consisting of 394 amino acids. EBP1 harbors an N-terminal and C-terminal polybasic (PBS) sequence. An overlapping putative Nucleolar localization signal (aa 357-358) with a lysine rich binding motif (364-RKTQKKKKKK-373) are found within the C-terminal PBS. The shared functional sequence between NoLS and lysine rich binding motif suggest dual functionality of the C-terminal binding motif. Four C-terminal motif mutations on EBP1; Q367H, Q367K, K373E-Ins, and K372R-Del, were discovered in various cancer tissues and the aim of this project was to investigate their effect on protein functionality. Mutations were generated in pEGFP-C2 and pGEX-4-T2 plasmids, which produced EGFP and GST tagged proteins.

The effect of mutations on the NoLS was investigated through an immunostaining localization experiment. This revealed a decrease in nucleolar localization for Q367K, while the K372R-Del mutation resulted in increased nucleolar localization as well as more nucleoli per cell. K373E-ins expressed localization pattern reminiscent of both Q367K and K372R-Del, while Q367H mutation appeared to not affect protein localization.

EBP1 was introduced to the group as a binding protein to the nucleolar signal molecule PtdIns(3,4,5)P_3. How the mutations influenced/affected the C-terminal binding motif was investigated through lipid overlay assay. Q367K mutation revealed stronger PPIn binding. The most likely explanation was that the mutation resulted in an expanded the lysine rich C-terminal binding motif, reducing its specificity, and increasing its electrostatic binding affinity to negatively charged lipid headgroups.

Lastly after investigating the mutations effect on localization and binding, the effect on protein stability was explored in a preliminary thermal denaturation assay. The mutations seemed not to be a factor for protein stability, perhaps due to the C-terminal already being a disorganized part of the protein. However, the K372R-Del mutant denatured nearly 2°C lower than WT, possibly displaying some influence on stability. A recent study has solved EBP1 structure when in complex with ribosome subunit80, suggesting that EBP1 ligand

binding might stabilize the C-terminal. A next explorative step would be to perform a denaturation assay probing the effect of PPIn binding on EBP1 WT. As well as if the mutations cause a change in stability compared to WT, when bound to PPIn.

1. Introduction

1.1 Polyphosphoinositides

1.1.1 Polyphosphoinositides structure

Polyphosphoinositides (PPIn) are lipid molecules, consisting of a diacylglycerol backbone, with two hydrophobic tails, often arachidonic acid (Figure 1). The glycerol backbone is linked to a sugar inositol headgroup with a phosphodiester linkage. The PPIn are derived from phosphatidylinositol (PtdIns), which have a total of three hydroxyl groups attached to the inositol ring on position 3, 4, and 5. The ring can be phosphorylated by kinases and dephosphorylated by phosphatases on the hydroxyl groups, giving rise to a total of seven unique polyphosphoinositides. Three monophosphorylated (PtdIns*3P*, PtdIns*4P*, PtdIns*5P*), three diphosphorylated (PtdIns(3,4)P_2, PtdIns(3,5)P_2, PtdIns(4,5)P_2) and a triphosphorylated (PtdIns(3,4,5)P_3) PPIn are derived from PtdIns (Balla, 2013; Raghu et al., 2019).

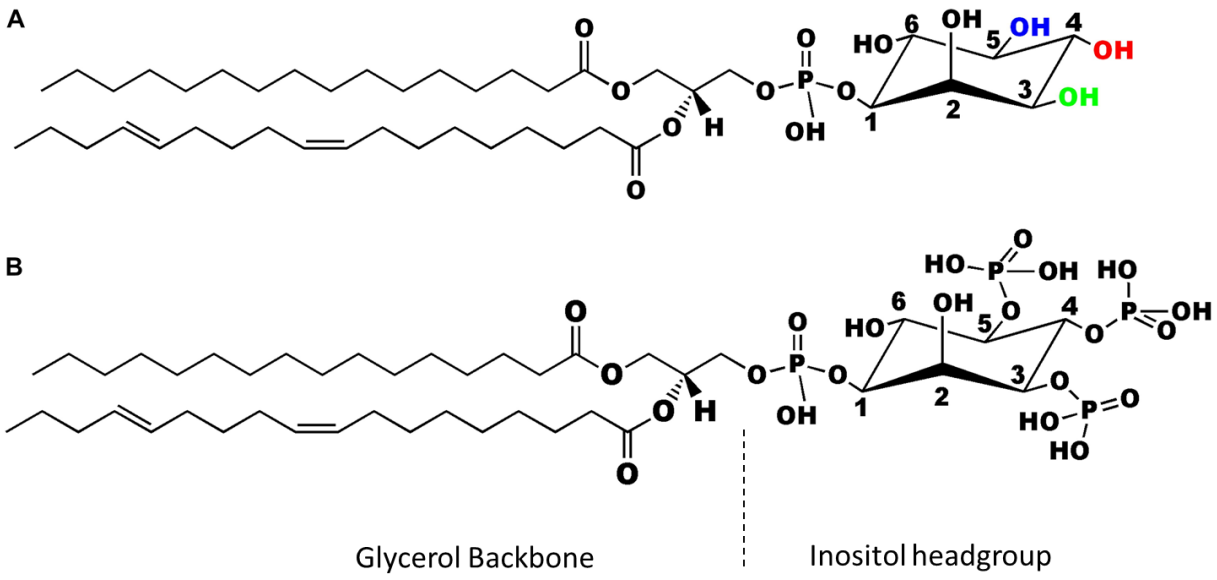

Figure 1. Chemical structure of polyphosphoinositides.
A) Phosphatidylinositol (PtdIns) consist of a glycerol backbone and an inositol headgroup. The inositol ring carries three hydroxyl groups on position 3 (green), 4 (red), and 5 (blue), available for phosphorylation. B) Phosphorylation of the hydroxyl groups, yield the polyphosphoinositide, phosphatidylinositol (3,4,5)-trisphosphate (PtdIns(3,4,5)P_3). Figure taken from (Raghu et al., 2019) and modified.

1.1.2 Polyphosphoinositides localization and metabolism

PPIn largely behave as signaling molecules and have been connected to copious sub-cellular processes, including membrane signaling and transport, cytoskeletal regulation, nuclear signaling and cell cycle regulation (De Craene et al., 2017; McCrea & De Camilli, 2009; Raghu et al., 2019). The main component of the bilayer plasma membrane are phospholipids such as phosphatidylcholine (PC), phosphatidylethanolamine (PE), phosphatidylserine (PS), sphingomyelin (SM), and PtdIns. About 10% of the plasma membrane consist of PtdIns, however the phosphorylated PPIn are low in abundance in the membrane, only 1%. are the phosphorylated PPIn (De Craene et al., 2017).

De novo synthetization of PtdIns transpire in the endoplasmic reticulum (ER), before subsequent transportation, by either transfer proteins or vesicles to target membranes, such as Golgi, lysosome and nucleus, where further refinement producing PPIn may take place. What cellular sub-compartments PPIn prefer to reside in, depends on the phosphorylation, PtdIns(4,5)P_2, PtdIns(3,4)P_2 and PtdIns(3,4,5)P_3 mainly localize in the plasma membrane, PtdIns(4)P in the Golgi complex as well as the plasma membrane, while PtdIns(3)P prefer to occupy the early endosome (Blunsom & Cockcroft, 2020; Gilbert Di & De Camilli, 2006; Viaud et al., 2016). PtdIns(4)P and PtdIns(4,5)P_2 are the most abundant PPIn making up approximately 10% of the PPIn composition (Viaud et al., 2016). Production of specific PPIn is strictly regulated by kinases and phosphatases (Figure 2) in response to both extra and intra cellular stimuli. The proteins and enzymes involved in PPIn metabolism are highly conserved(Raghu et al., 2019) The hydrolyzation of PtdIns(4,5)P_2 by phospholipase C (PLC) create two secondar messenger diacylglycerol (DAG), which among others activate protein kinase C (PKC). The other secondary messenger created inositol 1,4,5-trisphosphate (Ins(1,4,5)P_3), control Ca^{2+} flux (Payrastre et al., 2001; Tsui & York, 2010).

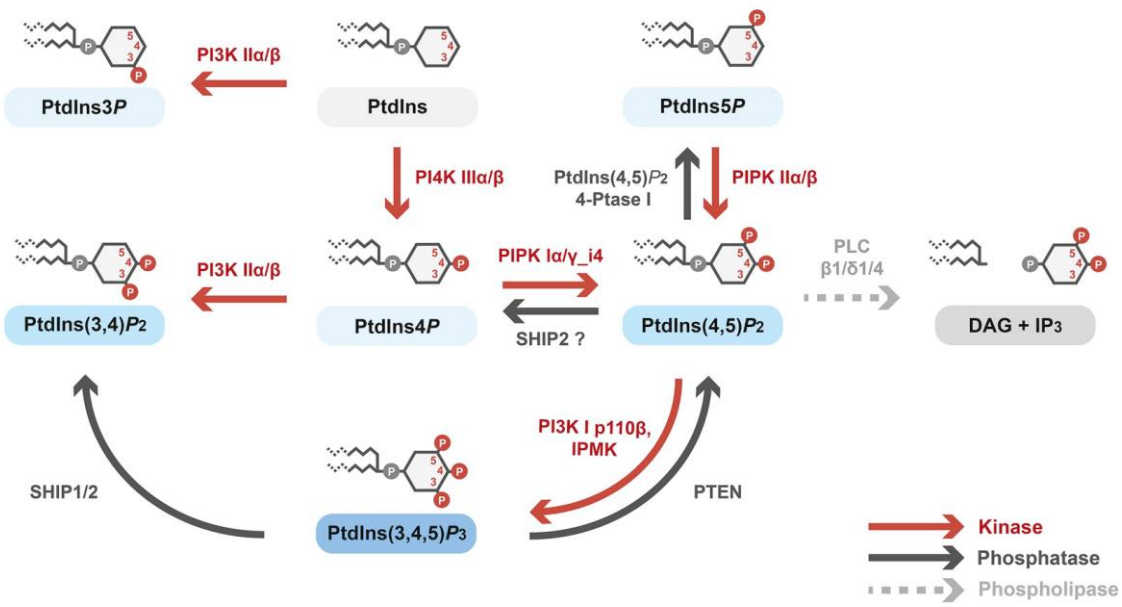

Figure 2. Polyphosphoinositide medtabolism.
A total of 7 different phosphoinositides can be produced through different kinase and phosphatase activities on phosphatidylinositol's (PtdIns) ring position 3, 4, and 5. Figure taken from (Jacobsen et al., 2019).

1.1.3 Polyphosphoinositide binding domains

The fatty acyl chains on PPIn are inserted into the membrane, while the charged headgroup protrudes from the membrane and allow for interactions with various proteins, when subjected to stimuli (Shah et al., 2013). PPIn signaling activity is often dependent on interactions with specific phospholipid binding domains. The most well known of which are pleckstrin homology (PH), 'Fab1, YOyoTB, Vac1, EE A1' (FYVE), PX and, and C1. Each domain has a distinct binding process with particular PPIn, ensuring the specificity of the domains (Lemmon, 2008). Additionally, PPIn have shown themselves willing to interact with electrostatic polybasic regions (PBS), such as K/R binding domains. Basic residues interact with negatively charged phosphate groups, furthermore hydrophobic interactions with lipid tails and PBS may occur (Hammond & Balla, 2015; Lewis et al., 2011). The C1 domains are zink finger domains, that are found in PKC and DAG kinesis. C1 domains target DAG and facilitate enzyme activity, phosphorylation and dephosphorylation (Colón-González & Kazanietz, 2006; Lemmon, 2008). The PH domain is found in phospholipase C-δ_1 (PLC), it bind stereospecifically to the PtdIns(4,5)P_2 and PtdIns(3,4,5)P_3 headgroup (Garcia et al., 1995;

Lemmon, 2008). FYVE domains are another type of Zink finger domain containing a hydrophobic binding pocket for binding of PtdIns(3)*P* headgroup, as well anchoring into the membrane. PtdIns(3)*P* also is the preferred ligand for the Phox-homology (PX) domain, but it interacts with PtdIns(3,4)P_2 or PtdIns(4,5)P_2 as well. PX domains are located on sorting nexin (SNX) protein and bind PPIn similar to FYVE (Lemmon, 2008).

1.1.4 Nuclear polyphosphoinositides

Some of the earliest discoveries regarding PPIn signaling ability constituted of observing PtdIns and PPIn turnover in brain cortex slices and pancreas upon stimulation (Hokin & Hokin, 1955). Since then PPIn signaling activity have been firmly established in a wide array of processes, including as an effector protein in the nucleus. Six of the seven PPIn have been discovered in preferred sub-nucleolar localizations. PtdIns(3)*P*, PtdIns(4)*P*, PtdIns(5)*P*, PtdIns(4,5)P_2, and PtdIns(3,4,5)P_3 locate to the nucleolus, and PtdIns(3,4)P_2, is only found in the nuclear membrane (Jacobsen et al., 2019). PtdIns(3,4,5)P_3 have also been found in the nuclear matrix, where it mediate apoptosis through PI3K and Nucleophosmin interactions (Jacobsen et al., 2019; Jee-Yin et al., 2004). PPIn are further capable of controlling apoptosis, through binding with the PH domain on Phosphatidylinositol 3 (PI3)-kinase enhancer (PIKE) and consequently inhibiting PIKE, which further prevents PI3K phosphorylation of nuclear Akt (Hu et al., 2005). PtdIns(4,5)P_2 pools have been found within nuclear speckles, in close proximity to phosphatidylinositol phosphate kinases (PIPK) producing said PPIn, as well as pre-mRNASuggesting possible PtdIns(4,5)P_2 processing of mRNA (Boronenkov et al., 1998). PtdIns(4,5)P_2 in the nucleoli interact and colocalize with RNA polymerase I (Pol I), upstream binding factor (UBF), and fibrillarin likely taking part in regulating rRNA processing, on top of that PtdIns(4,5)P_2 will take part in complexing with the active transcription machinery (Sobol et al., 2013; Yildirim et al., 2013). PPIn are also involved in regulating other nuclear processes as well, such as cell survival, cell cycle, chromatin remodeling, and splicing (Jacobsen et al., 2019; Lee et al., 2008).

1.2. Nucleolus

The nucleolus is a highly organized membrane less subcellular compartment within the cell nucleus, where synthesis, posttranscriptional modifications, and processing of rRNA

take place. The nucleolus consists of aggregated biomolecules, and is held together by their interactions in response to the cell cycle (Shaw & Brown, 2012). The nucleolus have a dynamic nature, as it alters shape, size, and placement in response to regulatory stimuli, as well as dissolve and rebuild during mitosis (Hernandez-Verdun, 2011; Shaw & Brown, 2012). Reformation of nucleoli often happens through initial formation of small nucleoli fusing into a larger nucleolus (Shaw et al., 1995). The initial creation of nucleoli occurs when rDNA transcription machinery cluster around specific chromosomal sites, called nucleolar organizer regions (NOR). Nucleolar biomolecules aggregate around the NOR as well forming the nucleoli (Raška et al., 2006; Roussel et al., 1996). The nucleolar biomolecular composition is also dynamic, proteins constantly move between cytosol and nucleoli (Shaw & Brown, 2012). Through electron microscopy, it was deduced the nucleoli was further subcompartmentalized into three defined sections, a fibrillar center (FC), dense fibrillar component (DFC), and granular component (GC) (Figure 3). FC is a small region within the nucleolus, lightly stained, where rDNA transcription happens. However, most rDNA transcription as well as early rRNA processing occur in DFC a densely packet region, surrounding FC. The major component of the nucleolus is the outer GC, harboring many different nucleolar complexes, including late rRNA processing and assembly with ribosomal proteins (Hernandez-Verdun, 2011; Shaw & Brown, 2012; Shaw et al., 1995).

The nucleolus is the main site of ribosome biogenesis (Shaw et al., 1995). Many different types of molecules aggregate in the nucleolus; ribosomal genes (rDNA), ribosomal RNA (rRNA), such as 47 subunit (47S) which are processed into smaller useful subunits. 18S, 5.8S, 28S as well as ribosomal proteins (Hernandez-Verdun, 2011; Raška et al., 2006). In addition to ribosome biogenesis, many other non-ribosomal activities occur in the nucleolus as well. Such as assembly of ribonucleoprotein and RNA processing by Signal recognition particle (SRP) (Pederson, 1998), telomerase assembly and regulation. Several miRNA are concentrated in the nucleolus both as precursors and in mature form in GC, possibly taking part in modification and processing of rRNA (Politz et al., 2009; Reyes-Gutierrez et al., 2014). Two small U6 RNA and U2 RNA associate with fibrillarin in the nucleolus and are submitted to 2'-*O*-ribose methylation posttranscriptional modification (Ganot et al., 1999; Pederson, 1998). Nucleophosmin is another example of a multifunctional nucleolar protein, it interacts with DNA and the p48 isoform of EBP1, which localizes in both cytoplasm and nucleoli and is

a well-known regulator of cell cycle progression and function as a nucleolar organizer (López et al., 2020; Squatrito et al., 2004b).

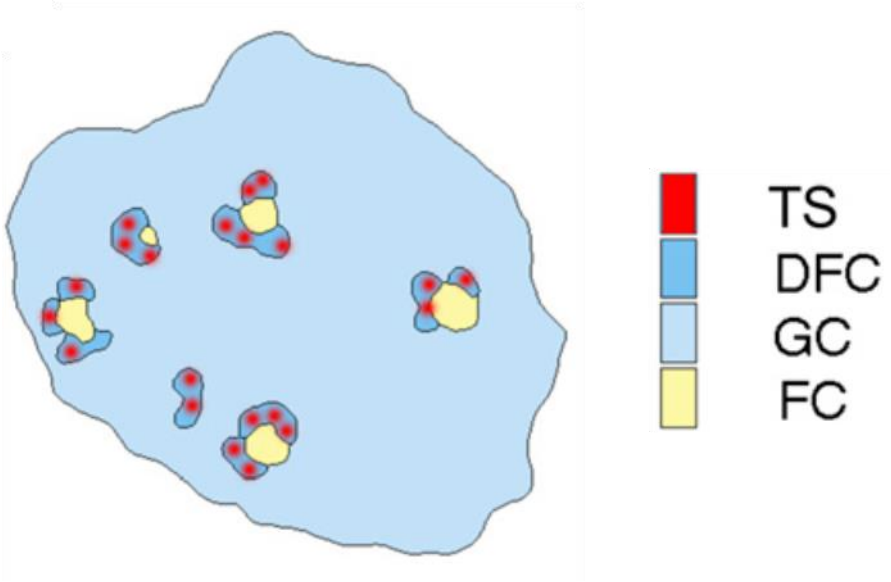

Figure 3. Nucleolus structure compartments.
Schematic of a nucleolus showing the different regions. The nucleolus is the main site for ribosome biogenesis and is organized into three distinct regions: fibrillar centers (FC), dense fibrillar component (DFC), and granular component (GC). Transcription sites (TS), where ribosome activity occurs are located within DFC. Figure modified from (Shaw & Brown, 2012).

1.3 ErbB3-binding protein 1

1.3.1 General about EBP1

ErbB3-binding protein 1 (EBP1) is an ubiquitously expressed protein (Lessor et al., 2000). EBP1 in humans is transcribed from the gene *PA2G4* located on chromosome 12q13.2 and contains ten exons (Lamartine et al., 1997). Two alternative EBP1 splicing products have been discovered, isoforms p48 and p42, with opposing functions in the cell, p42 is linked to tumor suppression, while p48 is linked to tumor development (Liu et al., 2006; Stevenson et al., 2020). *PA2G4* contains three in frame start codons (ATG→M, methionine). p48 is coded for from the first codon and is 394 amino acids long, however p42 starts at the third codon, located on exon 2 and lacks the first 54 amino acids (Lamartine et al., 1997).

EBP1 belongs to the M24 peptidase family, and its structure holds a conserved pita bread fold and a hydrophobic central cavity associated with methionine aminopeptidases (MAP) (Figure 4) (Kowalinski, Bange, Bradatsch, et al., 2007; Monie et al., 2007). The aminopeptidases are known for binding substrate, protein or peptide chains in the cavity and cleaving N-terminal amino acids. While the function of the central cavity in EBP1 is not fully understood, EBP1 does not possess aminopeptidase activity. The likely reason for lack of enzyme activity was revealed by juxtaposing the central cavity in hMAP with EBP1. A metal ion as well as amino acids 262-Asp, 399-His, and 459-Glu are necessary for hMAP catalytic function. In contrast the environment inside the EBP1 binding pocket is altered due to mutations of amino acids corresponding to hMAP, Asn-120, Asp-195 and Lys-320, in addition to loss of metal ion, likely rendering the binding pocket incapable of catalytic activity (Ball & Kaesberg, 1973; Monie et al., 2007; Taylor, 1993).

The full human EBP1 structure was solved when bound to 80S ribosome by cryo EM. The new structure is an important step forward, since this is the first instance where C-terminal EBP1-had been solved (Bhaskar et al., 2021). EBP1 was only partially solved in previous studies, due to the disorganized nature of the C-terminal (Kowalinski, Bange, Bradatsch, et al., 2007; Monie et al., 2007).

EBP1 is further distinguished from other MAPs through its extended N- and C-terminal (Kowalinski, Bange, Bradatsch, et al., 2007). The termini have both been identified as critical for proper EBP1 function through their three polybasic sequences (PBS) (Figure 5). The N-terminal region harbors two PBS in the shape of a lysine rich nuclear localization signal (aa K20-K22) and a lysine rich binding motif located on a loop (63-IFKKEKEMK-71). The two N-terminal motifs are located adjacent to each other in the structure, allowing for the possibility for the motifs to cooperate around their activity (Kowalinski, Bange, Bradatsch, et al., 2007). The C-terminal PBS (aa 301-394) serves several functions, most prominently it includes a lysine rich binding motif (364-RKTQKKKKKK-373) containing six continuous lysines (Squatrito et al., 2004b). The N- and C-terminal binding motifs follow the K/R motif K/R-($X_{n=3-7}$)-KXKK consensus sequence, and were shown to bind polyphosphoinositides through electrostatic interactions, the positively charged motifs attract negatively charged molecules (Lewis et al., 2011; Martin, 1998). A putative nucleolar localization signal (NoLS) (aa 357-385), was estimated for the C-terminal contributing another function to the region (Karlsson

et al., 2016; Squatrito et al., 2004b). Additionally, the C-terminal binding motif fold into a α-helix, containing an internal ribosome entry site IRES, which may interact with RNA (Bhaskar et al., 2021; Stevenson et al., 2020).

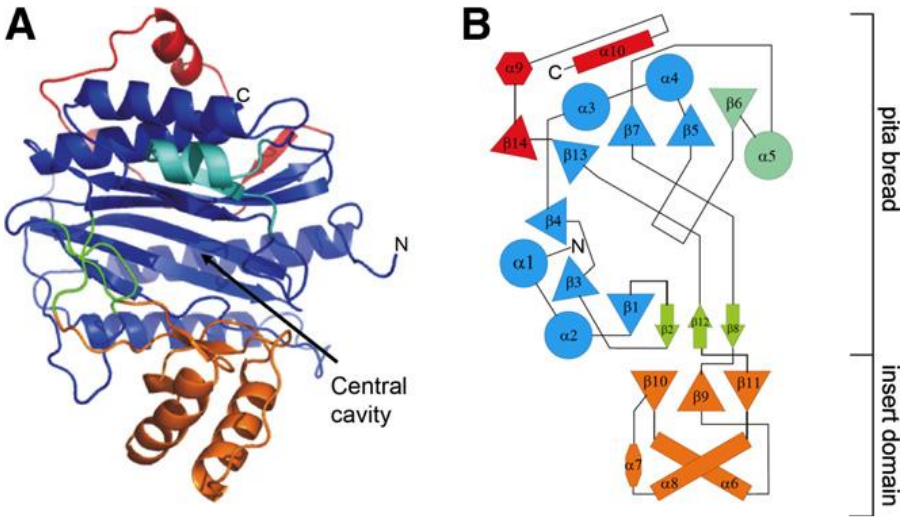

Figure 4. Early EBP1 structure.
Crystal structure of EBP1 (aa 7-362) showing a conserved methionine aminopeptidase structure, shaped like a pita bread structure with a central cavity, without any known catalytic function. Figure taken from (Kowalinski, Bange, Bradatsch, et al., 2007).

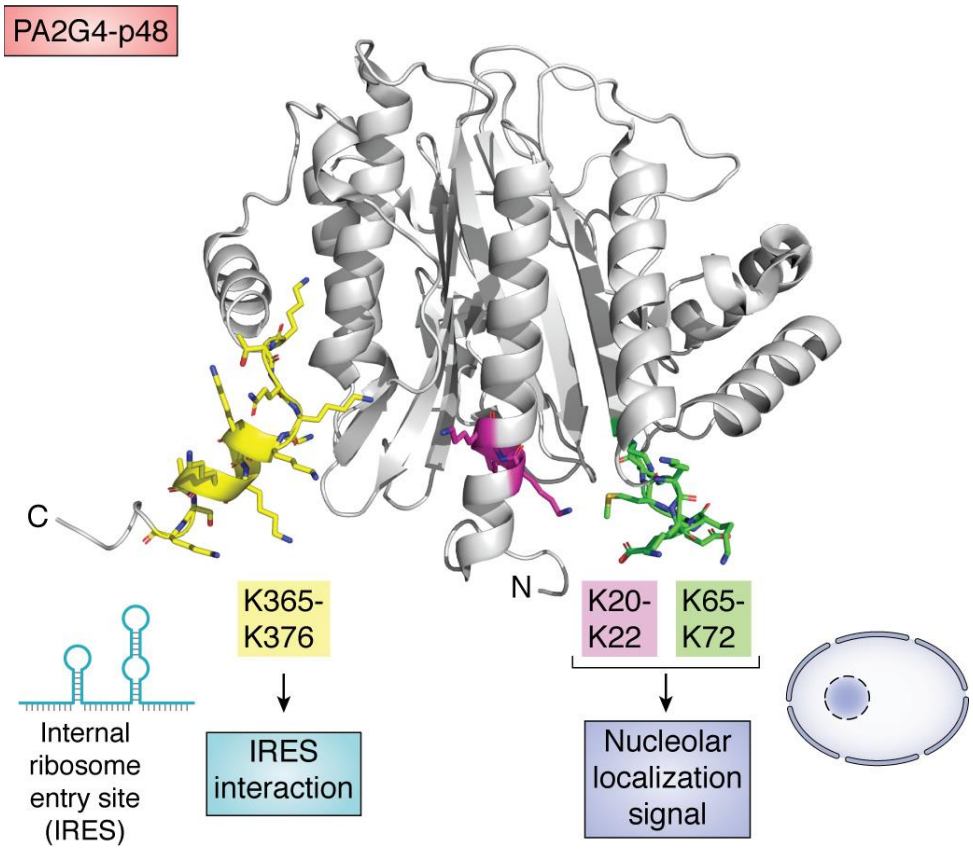

Figure 5. EBP1 contains several polybasic regions.
Full EBP1 structure showing the three main functional polybasic regions. A C-terminal binding motif (yellow) containing six consecutive lysine residues also expressing a nucleolar localization signal (NoLS) and an internal ribosome entry site (IRES). The N-terminal have two lysine rich areas, a nuclear localization signal (NLS) (Magenta) and a binding motif (green). Figure taken from (Stevenson et al., 2020).

1.3.2 EBP1 is a multifunctional protein with many binding interactions

EBP1 is an ubiquitously expressed multifunctional protein, involved in regulation of cell proliferation. EBP1 is highly conserved across species and much of the initial knowledge of human EBP1 has been deduced from its murine p38-2G4 homolog (Radomski & Jost, 1995). Nevertheless, EBP1 function and role is not well understood. The protein is known to interact with several biomolecules in the cell. EBP1 plays a part in regulating transcription and translation through interactions with many RNA molecules and proteins (Stevenson et al., 2020) Also, the nuclear lipid signaling molecules, PtdIns(4,5)P_2 and PtdIns(3,4,5)P_3 have been found to colocalize, bind, and interact with EBP1 in nucleoli (Karlsson et al., 2016; Lewis et al., 2011).

Through its various interactions, the two EBP1 isoforms, p42 and p48, have showcased opposing activity in the cell. Cell proliferation assays have revealed that p42-EBP1 has the ability to suppress and p48-EBP1 to induce cell growth (Liu et al., 2006). The different isoforms were present at different levels in cells dependent on the cell cycle phase. p48 influence on DNA synthesis and cell proliferation were further confirmed, due to p48 having increased levels of cells in the S phase compared to p42. (Liu et al., 2006).

The two isoforms also have different binding affinity as well as locate differently in the cells, the p42 isoform is mostly cytosolic, whereas p48 locates in the cytosol and nucleoli, 90% of cells transfected with p48 EBP1 located in nucleoli (Yan & Ziff, 1995). However, after treatment with nuclear growth factor (NGF), nucleolar localization was reduced to 20%. NGF treatment was shown to slow down cell proliferation, but not halt it completely through inhibition of Cdk kinases (Yan & Ziff, 1995). Likely the treatment caused EBP1 to relocate from nucleoli to the nucleoplasm. (Liu et al., 2006). P48 was shown to bind Akt in the nucleus (when treated with NGF), but not in the cytoplasm. P42 does not interact with nuclear Akt, and very little with cytoplasmic Akt (Liu et al., 2006). Bound p48 and Akt form complex with MDM2, which bind and ubiquitinated p53. P53 will be marked for degradation by proteasome, consequently inhibiting p53 tumor suppressor activity (figure 6) (Stevenson et al., 2020).

EBP1 was first identified as a binding protein to ErbB3, a tyrosine receptor kinase (Yoo et al., 2000). EBP1 was found to be a highly conserved human homolog to murine p38-2G4, a protein involved in cell cycle regulations (Lamartine et al., 1997; Yoo et al., 2000). EBP1 was shown to bind to ErbB3 and dissociate when in the presence of Heregulin (HRG), an ErbB3 ligand. The HRG binding of ErbB3 induced dimerization, phosphorylation and initiation of tyrosine kinase signaling (Goldman et al., 1990; Kim et al., 1994). Upon dissociation, EBP1, was reported to translocate to the nucleus, where it too will become phosphorylated. PKC upholds a basal level of EBP1 phosphorylation on Ser-360, which is necessary for its nucleolar localization (Lessor & Hamburger, 2001; Liu et al., 2006). The influence HRG and PKC have on EBP1 association with ErbB3, as well as phosphorylation is evidence of their role as likely EBP1 regulators, however the mechanisms with which this occur is not well understood (Lessor & Hamburger, 2001).

EBP1 also bind RNA and DNA, a possible way for EBP1 binding of RNA and DNA is through σ^{70} like sequence. Amino acids 46-64 on EBP1 show great homology with the σ^{70} motif consensus sequence, found in Imp4p proteins to bind nucleotides. The σ^{70} like motif was found to be necessary for EBP1 and RNA binding (Squatrito et al., 2004b). EBP1 was also identified as a RNA binding protein in RNA affinity chromatography and RNA co-immunoprecipitation assays (Bose et al., 2006).

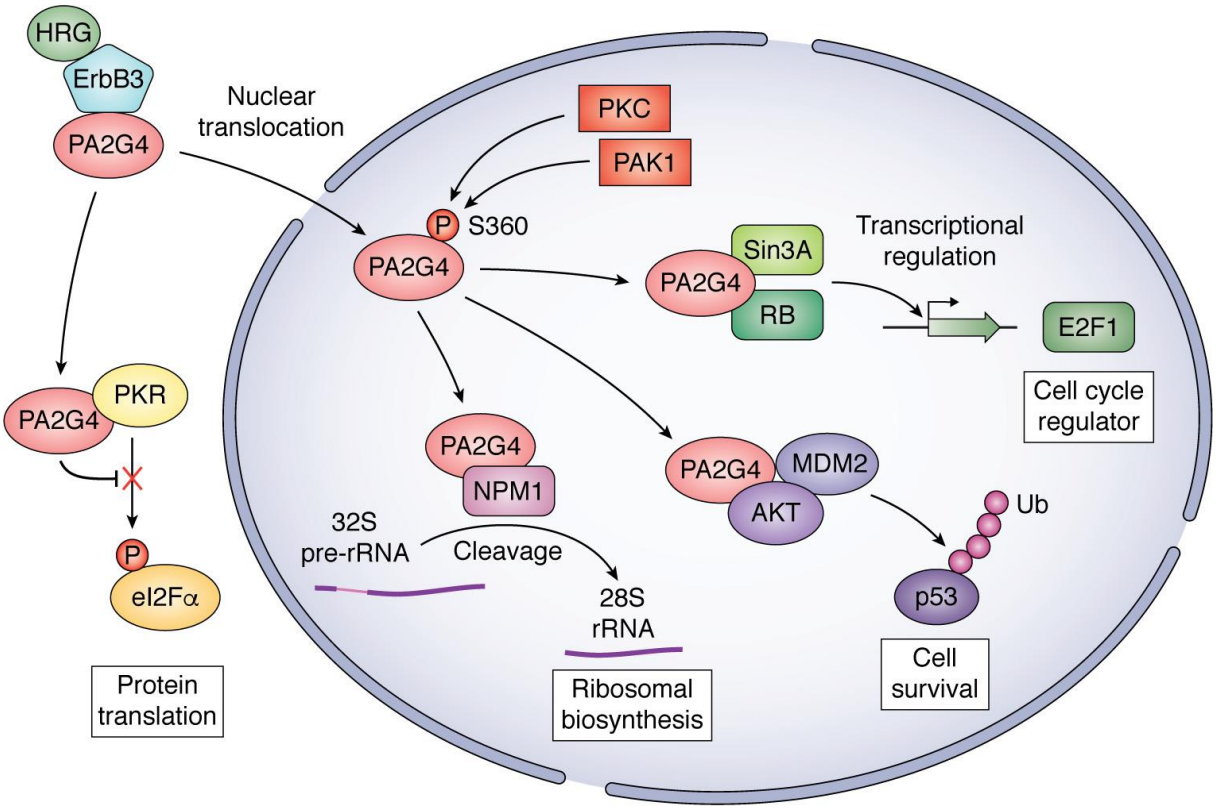

Figure 6. EBP1 is a multifunctional protein.
EBP1 is a ubiquitous protein regulating the cell cycle through different interactions with biomolecules in the cell both in the cytoplasm and nucleus (blue oval). Abbreviations: Heregulin (HRG), ErbB3 (ErbB3 tyrosine kinase), EBP1 (PA2G4), protein kinase C (PKC), p21-activated kinase (PAK1), eukaryotic initiation factor (eIF2α), dsRNA-activated kinase (PKR), Nucleophosmin (NPM1), E3 ubiquitin-protein ligase Mdm2 (MDM2), Retinoblastoma (Rb), Protein kinase B (Akt), ubiquitin (Ub), E2F1 transcription factor, and Paired amphipathic helix protein Sin3a (Sin3A). Figure taken from (Stevenson et al., 2020)

1.3.3 EBP1 association with 80S ribosome

In the last year, the first cryo EM structures of EBP1 bound to human 80S ribosome were reported (figure 7.) (Bhaskar et al., 2021; Wild et al., 2020). In these structures, EBP1

was shown to interact with its ribosomal insert domain, i.e. the residues 245-306 forming an alpha helix, and blocking the tunnel exit channel (Bhaskar et al., 2021). When EBP1 is bound to the ribosome it interacts and create a ribonucleoprotein complex, with several ribosomal proteins such as uL23, uL29 and eL19, as well as 28S rRNA. Upon binding, EBP1 also recruits ES27L, a large rRNA expansion segment in eukaryotic ribosome, responsible for proofreading and correct translation. ES27L behaves as an RNA scaffold and assists in EBP1 binding to the ribosome (Fujii et al., 2018). In return, EBP1 stabilize ES27L as well as facilitate various positions of the ES27L-B-arm. (Wild et al., 2020) EBP1 interacts with ES27L through two N-terminal alpha helixes in the conserved fold as well as the C-terminal (Bhaskar et al., 2021; Fujii et al., 2018; Kramer et al., 2002; Wild et al., 2020). The inhibitory effect of EBP1 blockage of the ribosome exit channel is yet to be deduced, but it appears to sterically hinder nucleocapsid (NC) from exiting the ribosome and in that way inhibit translation. EBP1 in complex with ribosome will also prevent phosphorylation of initiation factor eIF2α, by various protein kinases, which consequently will halt protein translation. EBP1 blockage will also obstruct binding of NAP or other MAPs to the tunnel exit, thus hindering co-translational modifications on forming peptide chains (Squatrito et al., 2006; Wild et al., 2020).

It has been suggested that p42 do not bind ribosomes as a consequence of lacking the first 54 residues. Noticeably, p48 interact with ribosomes through the insert domain before the C-terminal, residues 245-306 (Bhaskar et al., 2021). That being so, it is further suggested that p42 and p48 might have substantially different conformations dictating their function in the cells.

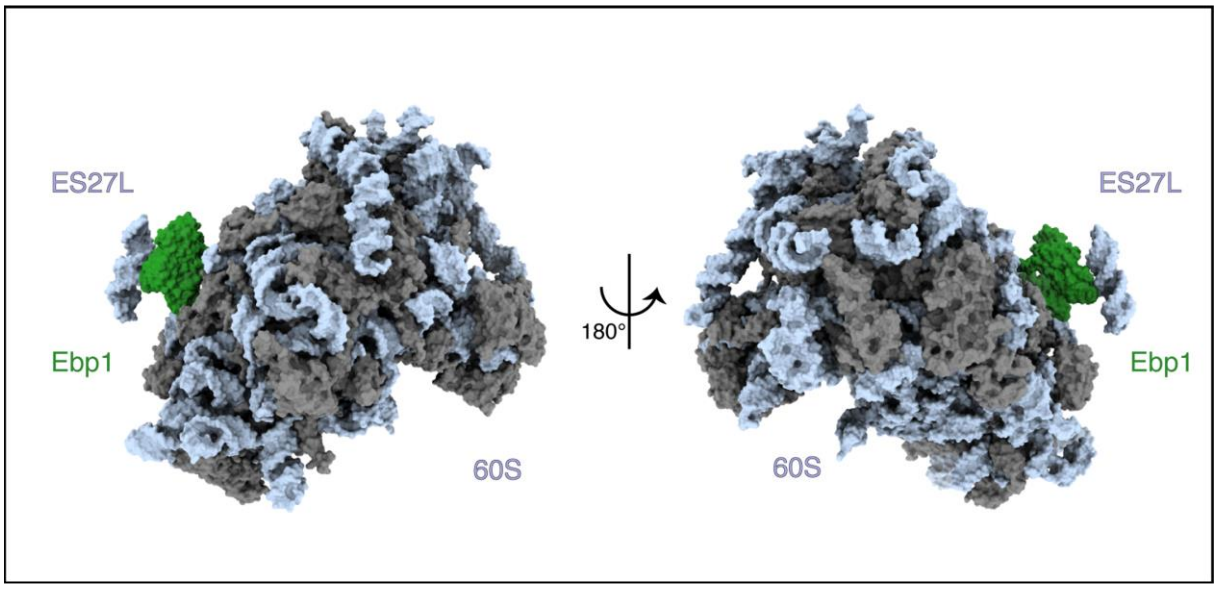

Figure 7. Full CRYO EM structure of EBP1.
The full p48 EBP1 structure (green) in complex with 60S ribosome and ES27L. rRNA in light blue and ribosomal proteins in gray**.** Figure modified from (Bhaskar et al., 2021).

1.3.4 Role of EBP1 in embryonic development

P48 EBP1, but not p42, plays a role in cell differentiation, this is demonstrated in several studies on EBP1 in embryonic development. EBP1 binds the DNMT1 promoter and inhibit transcription. Consequently, preventing DNMT1 from complexing with Suv39H and participate in gene silencing through histone methylation. In mouse knock out of EBP1 Suv39H1/DNMT1 complex is expressed thus promoting gene silencing of target gene, Survivin, a protein preventing apoptosis during embryonic development. Embryos from knock out were characterized by irregular development, pronounced cell death, and brain malformation (Kawamura et al., 2003; Ko et al., 2019). EBP1 also behaves as a cofactor when interacting with transcription factor SIX1. Knocked down EBP1 in Xenopus, lead to down-regulation of neural border zone, neural crest, and cranial placode genes (Neilson et al., 2017).

In another study the p48 isoform is present at high levels in satellite stem cells and myoblasts. Differentiation of myoblasts through myogenesis develop myocytes or muscles cells. When EBP1 is knocked down in mouse proliferation and differentiation is inhibited and abnormal development of the myotube. Additional, knockdown of EBP1 in chick embryos

result in resulted in inhibition of differentiation of muscle progenitors (Birbrair et al., 2013; Figeac et al., 2014).

Developmental Pluripotency-Associated-4 (DPPA4) in human embryonic stem cells bind p48 EBP1 through a SAF-A/B Acinus and PIAS (SAP) domain. However, EBP1 expression levels are decidedly reduced as cell differentiation progress. Also here EBP1 function as a co-factor to DPPA4 in transcriptional regulation of pluripotency (Somanath et al., 2018).

1.3.5 EBP1 in cancer

Aberrant EBP1 expression and behavior have long been connected with many types of cancer (Kim et al., 2012; Kim et al., 2010). High levels of EBP1 expression in primary breast cancer tumors, neuroblastoma, cervical cancer, prostate cancer, and acute myelogenous leukemia have been linked to poor survival prognosis in patients, further suggesting high EBP1 levels promote malignant neoplasia (Gannon et al., 2008; Koach et al., 2019; Liu et al., 2015; Nguyen et al., 2016; Ou et al., 2006).

1.3.6 P48 EBP1 in cancer

Overexpression of the p48 isoform induce malignant transformation of cells in human glioblastoma (GBM), represented by several cancer hallmarks; self-sufficient cell growth, cell proliferation trough increased clonogenicity, and tissue invasion. GBM tumors also show a relationship with EBP1 levels and patient survival, high EBP1 levels lowers the chance of survival (Hanahan & Weinberg, 2000; Kim et al., 2010).

P53 is a very commonly mutated protein in cancer. EBP1 was shown to be a regulator of p53 and loss of EBP1 control, affect p53 regulation, which may promote cancer development. P53 is a tumor suppressor protein, known to arrest the cell cycle (in G1 phase), when DNA damage is discovered. Following PKC-mediated phosphorylation of EBP1 on Ser-360, a complex is formed with MDM2 and phosphorylated Akt (Jee-Yin et al., 2006) (Figure 6). The complex was reported to bind p53, preparing it for ubiquitination and subsequent proteasomal degradation (Cui et al., 2020). EBP1 therefore inhibits p53 tumor suppressor function. Hence, EBP1 overexpression cause oncogenic behavior through increased p53 binding ensuing p53 degradation, and consequent loss of p53 induced cell arrest. (Im & Ham, 2020; Kim et al., 2012; Kim et al., 2010; Stevenson et al., 2020)

SKP1/CUL1/F-box protein (SCF) E3 ubiquitin ligase harbors a F-box and WD40 domain protein 7 (FBXW7) substrate receptor. P53 has been identified as a substrate that binds directly to the WD40 domain on FBXW7. This binding inhibits p53 tumor suppression activity, ubiquitinate p53 and promote degradation by proteasome (Cui et al., 2020; Wang et al., 2017). SCF E3 ubiquitin ligase was reported to have the same effect on p48-EBP1. When FBXW7 was present it could bind the N-terminal of p48 EBP1, ubiquitinate S40 and S44, marking the protein for degradation (Wang et al., 2017). Lower p48 EBP1 levels caused tumor suppression and apoptotic behavior (Wang et al., 2017). In addition, p48-EBP1 may induce cancer by controlling FBXW7 localization. P48 EBP1 binding to the WD40 domain also result in covering an NLS sequence located within the WD40 domain. FBXW7 also interacted with the p42 EBP1 isoform, oppositely with increased tumor suppression. The p42 isoform have a different structure from the p48, the loss of the 54 first amino acids also prevent the smaller isoform from ubiquitination by FBXW7. P42 prefer binding, when FBXW7 is already bound to a substrate or in a complex. Consequently, stabilizing the ubiquitination process, and induce protein degradation, in that way enhancing tumor suppressing ability (Wang et al., 2017).

1.3.7 P42 EBP1 in cancer

The p42 EBP1 isoform is known to bind different biomolecules than p48, in particular proteins involved in tumor suppressor activities, such as; ErbB-3 receptor, androgen receptor (AR), phosphatidylinositol 3-kinase (PI3K), and retinoblastoma (Liu et al., 2009; Stevenson et al., 2020; Wang et al., 2017; Xia et al., 2001; Zhang et al., 2002). A possible reason for different binding between isoforms may be due to the lack of the first 54 amino acids in p42-EBP1 causing distinct conformations between the two isoforms and exposing different motifs in p42. In addition, the N-terminal may be a participant in EBP1 stabilization, based on the p42 isoform having lower levels in cancers cells, compared to p48 (Hwang et al., 2020). The hBre1 E3 ubiquitin ligase can polyubiquitinate the p42 isoform, which has been believed the only isoform targeted for ubiquitination. However, p48 has been targeted by SCF E3 ubiquitin ligase in a study. Excessive polyubiquitination ensued by degradation has been identified as a way to diminish the p42 EBP1-mediated tumor suppression ability in cancer cells (Liu et al., 2009; Stevenson et al., 2020; Wang et al., 2017).

The mechanism by which the p42 promote tumor suppression is not well understood (Ko et al., 2014). Nevertheless the p42-EBP1 isoform has been found to inhibit PI3K, by binding to the cSH2 domain on the p85 regulatory subunit. P42-EBP1 and PI3K binding also promote p85 degradation, by recruiting HSP70/CHIP. The HSP70 chaperone recognize p85 as its substrate and the Ubox-dependent E3 ligase ubiquitinate p85, marking it for proteasome degradation. When p42 EBP1 is overexpressed p85 levels are reduced, showcasing how the short isoform function as a tumor suppressor (Ko et al., 2014).

Under normal conditions the p42-EBP1 isoform disassociates from ErbB3, travel into the nucleus and bind RB directly with its C-terminal residues 300-372. P42 EBP1, Rb binding inhibits transcriptional performance by the transcription factor E2F1 and lower cyclin E levels. E2F1 and cyclin E promotes oncogenesis which is combated by p42 tumor suppressor activity. However reduced p42 EBP1 tumor suppression is exhibited in breast cancer. Where lower levels of p42 disassociate from ErbB3, enter the nucleus and is capable of binding Rb (Nevins, 2001; Stevenson et al., 2020; Xia et al., 2001).

1.4 Project aims

Through nuclear lipid pulldown assay and mass spectrometry, EBP1 was identified as binding to PtdIns(4,5)P_2, a nuclear signaling lipid (Lewis et al., 2011). Our group decided to further investigate the functional properties of EBP1, demonstrating PPIn interactions through PBS. EBP1 contain several lysine rich motifs, a N-terminal motif (aa 65-72) and a C-terminal motif (aa 365-376), harboring six consecutive lysines (Karlsson et al., 2016). Previous studies have shown that EBP1 localizes in the nucleolus and demonstrated its nucleolar localization through the C-terminal part of the protein (aa 301-394) (Squatrito et al., 2004a). The C-terminal lysine rich motif is located within the localization sequence. Our group demonstrated the C-terminal motif's role in EBP1 nucleolar localization (Karlsson et al., 2016).

Several mutations on EBP1 have been associated with cancer (Figure 8). There are particularly four C-terminal mutations, located within the lysine rich binding motif, whose properties are of interest. Two missense mutations, Q367K and Q367H, one adding a seventh consecutive lysine another adding a positively charged histidine. There are two

truncating mutations, K373E-Ins, an insertion mutation, and K372R-Del, which is a deletion mutation (Cerami et al., Cancer Discov. 2012, and Gao et al., Sci. Signal. 2013, (Tate et al., 2018). Both frame shifts reduce the number of consecutive lysins in the motif, in addition they increase the positive charge of the shortened peptide chain.

This project strived to give a physiological characterization of the C-terminal mutations, by investigating the effect the C-terminal mutant have on protein functionality, specifically:

- If the increased positive charges in the C-terminal motif had an effect on EBP1 binding to PPIn on a lipid blot.
- If the mutations caused a change in protein stability, through fluorescence thermal denaturation assays.
- If the mutations in the C-terminal binding motif, affected the subcellular localization of EBP1, by immunostaining and microscopy.

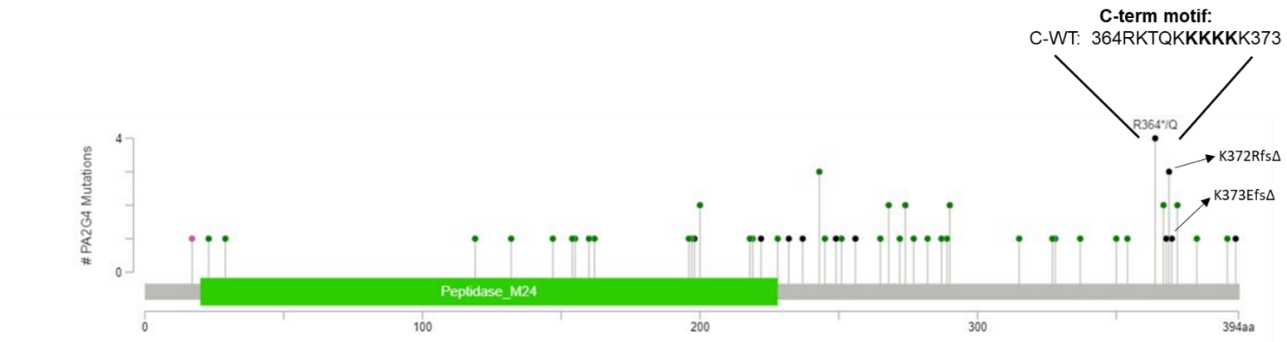

Figure 8. Overview over EBP1 mutations reported in cancer tumors.
A schematic representation of location and type of tumor mutation, identified in EBP1 from cancer tissue. The figure shows Q367H and Q367K missense mutations (green) and K373E-Ins and K372R-Del truncating mutations (Black) located at the C-terminal. *Figure adapted from cBioPortal.org 04 Dec 2020. Cerami et al., Cancer Discov. 2012, and Gao et al., Sci. Signal. 2013*

2 Materials

2.1 Chemicals, buffers, reagents, commercial kits, instruments and softwares

Table 2.1.1. Chemicals

Chemical	Abbreviation / Formula	Supplier
2-amino-2-hydroxymethyl-1,3- propanediol, Trizma® base	Tris	Sigma-Aldrich®
10% of 30% acrylamide/bisacrylamide (37.5:1)	30% acrylamide	BIO-RAD
4-(1,1,3,3-Tetramethylbutyl)phenyl-polyethylene glycol	Triton-X100	Sigma-Aldrich®
β-mercaptoethanol	β-met	
Agarose		Sigma- Aldrich®
Ammonium persulfate	APS	BIO-RAD
Ampicillin	Amp	Sigma-Aldrich®
Bacto Agar		Sigma-Aldrich®
Bovine serum albumin	BSA	Sigma-Aldrich®
Bovine serum albumin, essentially fatty acid free	FFA BSA	Sigma-Aldrich®
Dimethyl Sulfoxide	DMSO	Sigma-Aldrich®
Disodium hydrogen phosphate	$Na_2HPO_4x2H_2O$	Merck
DL-Dithiothreitol	DTT	Sigma-Aldrich®
Ethanol	EtOH	Kemetyl
Ethidium bromide	EtBr	Sigma-Aldrich®
Glycerol (UltraPure™)	glycerol	Invitrogen™
Hydrochloric acid	HCl	Sigma-Aldrich®
Isopropanol		Kemetyl
Isopropyl β-D-thiogalactopyranoside	IPTG	Apollo Scientific
Kanamycin sulfate	Kan	Sigma-Aldrich®
L-glutathione, reduced		Sigma-Aldrich®
Lysozyme		Sigma-Aldrich®
Milli-Q water	Milli-Q	
Monopotassium phosphate	KH_2PO_4	Sigma-Aldrich®
N,N,N',N'-tetramethyl-ethane-1,2-diamine	TEMED	BIO-RAD
Nonidet® P 40 Substitute	NP-40	Thermo Fisher Scientific
Paraformaldehyde	PFA	Merck
Polyoxyethylenesorbitan monolaurat	Tween-20	Sigma-Aldrich®
Potassium chloride	KCl	Merck
Sodium chloride	NaCl	Sigma-Aldrich®
Sodium hydroxide	NaOH	Merck
Titriplex® ethylenedinitrilotetraacetic acid disodium salt dehydrate	EDTA	Merck
tris(2-carboxyethyl)phosphine	TCEP	
Tryptone		Bacto™

Yeast extract	Bacto™

Table 2.1.2. Ready made buffers and reagents

Name	Purpose	Supplier
0,5 M Tris-HCl pH 6,8	SDS PAGE	BIO-RAD
1,5 M Tris-HCl pH 8,8	SDS PAGE	BIO-RAD
10x Tris/Glycine/SDS Buffer	SDS PAGE	BIO-RAD
10x Tris acetate EDTA (TAE) pH 7.6	Agarose gel electrophoresis	UiB lab
Big dye v.3.1	DNA sequencing	Thermo Fisher Scientific
cOmplete, EDTA-free, Protease Inhibitor Cocktail tablets	Cell lysis	Roche Diagnostics
DpnI restriction enzyme	Template DNA removal	New England BioLabs Inc.
Gel Loading Dye, Purple (6X)	Agarose gel electrophorese	New England BioLabs Inc.
Glutathione Sepharose™ 4 Fast Flow	Affinity chromatography	GE Healthcare
Goat serum	Blocking	Invitrogen™
InstantBlueTM Protein stain	SDS PAGE	Expedon
OPTI-MEM® | (1X) Reduced Serum Medium	Transfection	gibco
ProLong™ Glass Antifade Mountant with NucBlue™ Stain (hoechst)	Mounting cell slides	Invitrogen™
Protein Assay Dye Reagent Concentrate	Bradford reagent	BIO-RAD
S.O.C. medium	Transformation	Thermo Fisher Scientific
SDS Solution 20 % (w/v)	SDS PAGE	BIO-RAD
Sequencing buffer	DNA sequencing	Thermo Fisher Scientific
Thrombin	GST cleavage	GE Healthcare

Table 2.1.3. Commercial Kits

Name	purpose	Supplier
Lipofectamine® 3000 Transfection Kit	Transfection	Invitrogen™
Nucleospin® Gel and PCR Clean-up kit	PCR consentration	Macherey-Nagel
Phusion High-Fidelity DNA Polymerase kit	PCR STM	Thermo Fisher Scientific
PipStrips	Lipid overlay assay	echelon
Plasmid DNA purification kit	MiniPrep	Macherey-Nagel
Plasmid DNA purification NucleoBond® Xtra Midi kit	MidiPrep	Macherey-Nagel
SuperSignal™ West Pico PLUS Chemiluminescent Substrate kit	Lipid overlay assay	Thermo Fisher Scientific

PCR=polymerase chain reaction, STM=site directed mutagenesis

Table 2.1.4. Instruments

Name	Purpose	Manufacturer
Allegra® X-15R Centrifuge	Centrifugation	Beckman Coulter
Avanti® J-26 XP	High speed and high volume centrifugation	Beckman Coulter
ChemiDoc™ XRS+	Lipid blot imaging	BIO-RAD
Epoch Microplate Spectrophotometer	DNA and Protein concentration	BioTek
Fluorescence microscope DMI 6000 B	Immunostaining imaging	Leica
GelDoc™ EZ imager	Agararose gel and SDS-PAGE imaging	BIO-RAD
GenAmp® PCR System 2700	PCR	Applied Biosystems
Mini LabRoller Dual Format Rotator	Gentle mixing	Labnet
NanoDrop ND-1000™ Spectrophotometer	DNA and protein concentration	Saveen-Werner
Ultrospec 10 Cell density meter	Bacterial OD	Amersham Biosciences
ÄKTA™ Laboratory-scale Chromatography System	SEC chromatography	GE Healthcare Life Sciences

PCR=polymerase chain reaction, OD=optimal density

Table 2.1.5. Softwares

Name	Purpose	Developer
ApE- a plasmid editor (v. 2.0)	DNA sequences	M. Wayne Davis
Microsoft Excel	Data processing, figures, histograms and tables	Microsoft
Gen5	Epoch Microplate Spectrophotometer software	BioTek
Image J	Picture processing, lipid blot quantification	National institute of Health
Image Lab	Agarose gel, SDS-PAGE, Lipid blot imaging	BIO-RAD
Leica Application Suite X 3.7.4.23463	Immunostaining Imaging	Leica Microsystems
Sigmaplot	Denaturation curve	Sigma-Aldrich

2.2 PCR primers and plasmid acquisition

Table 2.2.1. Primers

Oligo nucleotide description	5’ – 3’ sequence	Purpose
EGFPC2 Rev	GGACAAACCACAACTAGAATGCA	Sequencing
PGE4T reverse Primer	CCTCTGACACATGCAGCTCCCG	Sequencing
Fwd Q367H	GTCGAAAAACC**CAC**AAAAAG	Point mutation
Rev Q367H	CTTTTT**GTG**GGTTTTTCGAC	Point mutation
Fwd Q367K	GTCGAAAAACCA**AG**AAAAAG	Point mutation
Rev Q367K	CTTTTT**CT**TGGTTTTTCGAC	Point mutation
Fwd K373E-Ins	CCCAGAAAAAGAAAAAAAAA**A**GAAGGCCTCC	Frameshift, Insertion mutation
Rev K373E-Ins	GGAGGCCTTC**T**TTTTTTTTCTTTTTCTGGG	Frameshift, Insertion mutation
K372Rfs-Del _fwd	CCCAGAAAAAG_AAAAAAA_GAAGGCCTCC	Frameshift, Deletion mutation
K372Rfs-Del _rev	GGAGGCCTTC_TTTTTTTCTTTTTCTGGG	Frameshift, Deletion mutation

Table 2.2.2. Plasmids

Name	Procurement	Abbreviation
pGEX-4T-2-FL-EBP1-WT	Readymade: EBP1 cloned into pGEX-4T-2	pGEX-EBP1 wt
pGEX-4T-2-FL-EBP1-Q367H	PCR STM	pGEX-EBP1-Q367H
pGEX-4T-2-FL-EBP1-Q367K	PCR STM	pGEX-EBP1-Q367K
pGEX-4T-2-FL-EBP1-K372R-Ins	PCR STM	pGEX-EBP1-Ins
pGEX-4T-2-FL-EBP1-K373E-Del	Readymade: PCR STM	pGEX-EBP1-Del
pEGFP-C1	Empty vector	
pEGFP-C2-FL-EBP1-WT	Readymade EBP1 cloned into pEGFP-C2	pEGFP-EBP1 wt
pEGFP-C2-FL-EBP1-Q367H	PCR STM	pEGFP-EBP1-Q367H
pEGFP-C2-FL-EBP1-Q367K	PCR STM	pEGFP-EBP1-Q367K
pEGFP-C2-FL-EBP1-K373E-Ins	Readymade: PCR STM	pEGFP-EBP1-Ins
pEGFP-C2-FL-EBP1-K372R-Del	Readymade: PCR STM	pEGFP-EBP1-Del

PCR=polymerase chain reaction, STM=site directed mutagenesis

2.3 Protein expression and purification

Table 2.3.1. LB medium and agar

LB medium	LB agar
1% (w/v) tryptone	1.5% (w/v) agar in LB medium
0.5% (w/v) yeast extract	
1% (w/v) NaCl	

Table 2.3.2. Lysis buffer

Stock	Lysis buffer
250mM NaCl	250mM NaCl
50mM Tris-HCl pH 7.5	50mM Tris-HCl pH 7.5
2mM EDTA pH 7.5	2mM EDTA pH 7.5
	0.5mM β-mercaptoethanol
	1mg/mL lysozyme
	4.6% (v/v) Glycerol
	2% (v/v) NP-40
	1tablet/50mL complete, EDTA-free, Protease Inhibitor Cocktail tablets

Table 2.3.3. Elution buffer.

Elution buffer
50mM Tris-HCl pH 8.0
150mM NaCl
0.5mM β-mercaptoethanol
0.03g/10mL reduced glutathione

Table 2.3.4. Wash buffer

Wash buffer
50mM Tris-HCl pH 8.0
100mM NaCl

2.4 Gel electrophoresis

Table 2.4.1. 10% SDS PAGE gels.

10% resolving gel	4% stacking gel
10% of 30% acrylamide/bisacrylamide (37.5:1)	5% of 30% acrylamide/bisacrylamide (37.5:1)
375 mM Tris-HCl pH 8.8	125 mM Tris-HCl pH 6.8
0.1% (v/v) SDS	0.1% (v/v) SDS
0.1% (v/v) APS	0.1% (v/v) APS
0.04% (v/v) TEMED	0.1% (v/v) TEMED

Table 2.4.2. Sample buffers

5x SDS sample buffer	6x DNA sample buffer

5% SDS (v/v)	1x TAE
5% SDS (v/v)	30% Glycerol
20% glycerol (v/v)	0.025% Bromophenol Blue
250 mM DTT	
0.2% Bromophenol blue (w/v)	

Table 2.4.3. Gel electrophoreses ladders

Name	Purpose	Supplier
2-log DNA ladder (0.1-10.0 kb)	Agarose gelelectrophorese	New England BioLabs Inc.
Precision Plus Protein™ Dual Color Standards	SDS-PAGE	BIO-RAD

2.5 Lipid blot

Table 2.5.1. Blocking buffer lipid blot

TBS-T	Blocking buffer
TBS	3% (w/v) essential fatty acid free BSA in TBS-T
1% (v/v) Tween-20	

2.6 Bacterial Strains

Table 2.6.1. Bacterial Lines

Name	Purpose	Supplier
XL1-Blue Supercompetent	Plasmid propagation after SDM	Agilent Technologies
XL1-Blue Homemade	Plasmid propagation after Mini/MidiPrep	*Andrea Papdiné Morovicz*
BL21DE3-CodonPlus	Protein expression	Agilent Technologies

SDM: site directed mutagenesis

2.7 Protein stability assay

Table 2.7.1. Size exclusion running buffer

Running buffer
50mM Tris-HCl pH 8
400mM NaCl
0.05mM TCEP added after elution

The buffer was degassed before use

2.8 Cell Work

Table 2.8.1. Solutions and buffers for cells work.

10x PBS pH 7.4	1x PBS	PFA	Blocking buffer	New Blocking buffer	Permeabilization solution	Washing buffer
1.37M NaCl	900mL Milli-Q	3.7% Paraformald-ehyde in 1x PBS	5% goat serum	3% free fatty acid BSA,	0.25% Triton-X100 in 1x PBS	0.1% Tween-20 in 1x PBS
27mM KCl	100mL 10xPBS		0.05% Triton-X100	0.05% Triton-X100		
100mM Na_2HPO_4	Autoclave before use		in 1x PBS	in 1xPBS		
18mM KH_2PO_4						
NaOH until pH 7.4						
Autoclave before use						

Table 2.8.2. Cell Lines.

Name	Type	Supplier
AU565	Breast Cancer cell line	Dr Elisabet Ognedal Berge, Klinisk institutt 2, UiB.

Table 2.8.3. Cell culture reagents

Name	Abbreviation	Supplier
Roswell Park Memorial Institute-1640 medium	RPMI-1640	SIGMA-ALDRICH
Fetal bovine serum	FBS	SIGMA-ALDRICH
Phosphate-buffered saline	PBS	Homemade
100 x Penicillin-Streptomycin	PS	SIGMA-ALDRICH
0.25% Trypsin-EDTA solution	Trypsin	SIGMA-ALDRICH
Dimethyl sulfoxide	DMSO	SIGMA-ALDRICH

2.9 Antibodies

Table 2.9.1. Antibodies

Antibody	Type	Species	Dilution	Application	Supplier	Cat. No
Fibrilliarin (C13C) mAb Rabbit	Primary	Rabbit	1:500	IF	Cell signalling technology	2639S
Nucleolin (C13C) mAb Rabbit	Primary	Rabbit	1:400	IF	Cell signalling technology	14574S
Alexa Fluor™ 594 goat anti-rabbit IgG (H+L)	Secondary	Goat	1:200	IF	Thermo Fisher Scientific	A11012
Rabbit Anti-GST-HRP	secondary	Rabbit	1:50000	LOA	abcam	Ab3416

IF= Immunofluorsecence, LOA= Lipid overlay assay

3 Methods

3.1 Plasmid acquisition

3.1.1 Site directed mutagenesis

pGEX-4T-2-EBP1 WT and the pEGFP-C2-EBP1 WT plasmids were used to generate Q367H, Q367K and K373E-Ins point mutations, using a Phusion High-Fidelity DNA Polymerase kit from ThermoScientific for the Q367H and Q367K mutations, and Turbo DNA polymerase from Agilent for the K373E-Ins mutation. The primers for the reactions (Table 2.2.1.), were designed to harbor the desired point mutations. The PCR reactions had a total reaction volume of 50 µL, consisting of Rxn buffer, 0.6 mM dNTP mix, 3% DMSO, 25-30ng template plasmid, 0.1 µM forward and reverse primer (Table 2.2.1.) 50 mM $MgCl_2$ was added to the Q367H and Q367K mutation reaction in addition to 2U Phusion DNA polymerase. K372R-Ins however was amplified by 2.5 U Pfu Turbo DNA polymerase. The reactions were executed, following the PCR program in 3.1.1 To remove template DNA, the remaining PCR product was digested with 10 U DpnI restriction enzyme for 2 h at 37°C.

Table 3.1.1. PCR program, for point mutations

Mutation	Program			
	Phase	Temperature	Time	Cycles
	Initial Denaturation	95°C	1 min	1
	Denaturation	95°C	1 min	20

K373E-Ins	Primer Annealing	55°C	1 min	20
	Elongation	68°C	8 min	20
	Final Elongation	68°C	7 min	1
	End	10°C	∞	1
	Initial Denaturation	98°C	40 sec	1
	Denaturation	98°C	10 sec	20
Q367H	Primer Annealing	50°C/57°C	30 sec	20
Q367K	Elongation	72°C	4 min 30 sec	20
	Final Elongation	72°C	7 min	1
	End	10°C	∞	1

Q367H use annealing temperature 50°C and Q367K use annealing temperature 57°C.

3.1.2 Agarose gel electrophoresis

Confirmation of plasmid amplification was carried out by running 10% of the PCR reaction product mixed with DNA loading buffer on an agarose gel (1% Agarose in Tris acetate EDTA (TAE) buffer pH 7.6) stained with 0.5 µg/mL ethidium bromide (EtBr). The gel was loaded with 5 µL 2-log DNA ladder and run at 95 Volts for 30-45 min. Gel imaging was conducted with GelDoc™ EZ Imager from BioRad.

3.1.3 PCR purification

To increase the effectiveness of transformation, DpnI digested PCR plasmid product was concentrated through a PCR purification process. This was done by using the protocol from Nucleospin® Gel and PCR Clean-up kit from Macherey-Nagel.

3.1.4 Transformation

The PCR product was transformed into XL1-Blue Supercompetent cells from *QuickChange Agilent technologies* in order to amplify the plasmid. 50 µL cells and 4.5 µL PCR purified plasmid were mixed and left to incubate on ice for 30 min. The cells were heatshocked for 45 sec, at 42°C and placed on ice for 2 min. 80 µL SOC medium, preheated to 37 °C were added to the cells and they were left to recover at 37°C, while shaking at 300 rpm, for 1 hour. The cells were plated on LB-agar plates containing antibiotics, dependent on the plasmid's resistance gene, 100 µg/mL Ampicillin for the pGEX-4T-2 vector or 50 µg/mL Kanamycin for the pEGFP-C2 vector. The cells were incubated overnight at 37°C, the following day the bacterial colonies were picked for inoculation for MiniPrep, MidiPrep.

3.1.5 Storing plasmids in glycerol stock

Plasmids can be stored in transformed bacteria for years in glycerol stock, at -80°C. A 15% glycerol stock was made by mixing 850 µL of O/N bacterial culture (see DNA MiniPrep and MidiPrep) in LB medium and Ampicillin (100µg/mL) or Kanamycin (50 µg/mL), with 150 µL 99% glycerol.

3.1.6 DNA MiniPrep and MidiPrep

DNA was mass produced from XL1-Blue Supercompetent cells transformed with the recombinant DNA constructs. A colony of each construct was picked for inoculation of MiniPrep or MidiPrep culture. For MiniPrep plasmid production a colony was transferred to 5 mL LB medium with antibiotics (100 µg/mL ampicillin or 50 µg/mL kanamycin), at 37°C, while shaking at 250 rpm, O/N. A Plasmid DNA purification kit from Macherey-Nagel was used for the purification.

When preparing for MidiPrep, 1mL LB broth with antibiotics (100 µg/mL ampicillin or 50 µg/mL kanamycin) was inoculated with a colony. The culture incubated at 37°C, while shaking at 250 rpm for 7 hours. A 100 mL culture was inoculated from the small culture, and incubated at 37°C, while shaking at 250rpm O/N. In the morning, a NucleoBond® Xtra Midi kit from Macherey-Nagel was used for MidiPrep purification. The MiniPrep and MidiPrep DNA concentrations were measured with Epoch microplate spectrophotometer.

3.1.7 DNA Sequencing

After the MiniPrep purification, the plasmid was DNA sequenced by Sanger sequencing, to ensure the correct mutation had occurred. First the sequence fragment where the mutation should be located was amplified by PCR, following the reaction scheme, 10 µL total reaction volume, with approximately 400 ng plasmid, EGFPC2 Rev or PGE4T reverse Primer (Table 2.2.1.), Sequencing buffer, and 1 µL Big Dye 3.1. The reaction was performed using the PCR program in 3.2.1. After the reaction, 10 µL Milli-Q water was mixed with the PCR product, before it was sent to the sequencing facility (UiB) for sequencing.

Table 3.1.2. PCR program, for sequencing

Program

Phase	Temperatur e	Time	Cycles
Initial Denaturation	96°C	5min	1
Denaturation	96°C	10sec	27
Primer Annealing	50°C	5sec	27
Elongation	60°C	4min	27
Final Elongation	4°C	7min	1
End	10°C	∞	1

3.2 Protein expression and purification

3.2.1 Expression and purification of protein in BL21 cells

Plasmids encoding EBP1 constructs were transformed in BL21-DE3 codon plus and plated on Ampicillin containing LB-agar plates. A colony was picked from the agar plate and inoculated in 5 mL LB broth, with Ampicillin(100 µg/mL) and incubated at 37°C, at 250 rpm, O/N. 100 mL LB broth, with Ampicillin (100 µg/mL), was inoculated the following morning with 2 mL of starter culture and incubated for 2-3 hours. Cultures were induced when A_{600} reached 0.7 with 0.5 mM Isopropyl β-D-thiogalactopyranoside (IPTG), and grown further at 37°C, 250 rpm, for 3 hours. The cultures were centrifuged at 3200 g for 15 min, the supernatant discarded, and the pellet stored at -80°C,

Pelleted bacteria were thawed and lysed on ice, in 10 mL lysis buffer (0.5 mM β-mercaptoethanol, 1 mg/mL Lysozyme, 4.6% (v/v) Glycerol, Protease Inhibitor Cocktail, 2% NP-40), The pellet was further lysed through sonication 5x, at 50% amplitude, 30 sec pulse on and 30 sec pause/off. The solution was then centrifuged at 18000 g for 40 min, the supernatant was collected and kept on ice for purification, 3mL Glutathione Sepharose beads were loaded on Econo-Pac® Chromatography Column and washed in 15 mL wash buffer (50 mM Tris-HCl pH 8.0, 100 mM NaCl). The Supernatant was added to the beads and left to bind at 4°C, while gently shaking, O/N. The first flowthrough was collected and stored at -80°C, for further protein extraction. The beads were then washed four times, in 10 mL ice cold PBS and once in wash buffer, and subsequently incubated with 3 mL elution buffer (50 mM Tris-HCl pH 8.0, 150 mM NaCl, 0.5 mM β-mercaptoethanol, 0.03 g/10mL reduced glutathione), on ice, while gently shaking for 30 min. The protein was eluted, the

concentration measured with NanoDrop™ 1000, the highest yields were pooled, aliquoted and stored at -80°C. A Bradford assay was done to find the accurate protein concentration and confirmed with a parallel protein SDS-PAGE gel.

3.2.2 GST cleavage on Sepharose beads

GST tagged EBP1 proteins were expressed as previously detailed. After O/N protein binding to the Sepharose beads, the beads were washed 4x, in 10 ml, ice cold PBS and once in wash buffer. The cleavage of GST from the EBP1 constructs was performed by adding 125 U thrombin at RT, while shaking, O/N. The protein was eluted after cleavage and stored at 4°C until further purification by size exclusion chromatography (SEC) on ÄKTA.

3.2.3 Size Exclusion chromatography

Thrombin and other remaining contaminants were separated from the GST cleaved EBP1 constructs through SEC purification on ÄKTA Explorer system, with UNICORN program. A HiLoadTM 16/600 SuperdexTM 75 pg column was used for the separation. The column was equilibrated with degassed running buffer (50 mM Tris-HCl pH 8, 400 mM NaCl, 0.05 mM TCEP) O/N. The GST-cleaved protein sample was loaded on the column. 500 µL fractions were collected and their protein concentration estimated by Bradford assay. To assess the purity, the protein fractions were run on 10% SDS-PAGE. The purified proteins were concentrated to a minimum of 400 µM by centrifugation at 3200 g for 17 min using Amicon Ultra 30 columns.

3.2.4 Bradford assay

The protein concentration for EBP1 constructs was determined by Bradford colorimetric assay. A Bovine Serum Albumine (BSA) standard, with BSA dilution concentrations 0.1 mg/mL, 0.25 mg/mL, 0.5 mg/mL, 0.74mg/mL, 1 mg/mL, 2.5 mg/mL, 5 mg/mL, and 7.5 mg/mL was prepared in elution buffer. 2 µL BSA standard and eluted protein, were pipetted in triplicates in 96 well plate. 200 µL Bradford reagent (diluted 1:5 and filtered) was added and pipetted up and down once, for mixing. The samples were left to incubate at RT for 5 min, before the absorbance was measured at 595 nm using Epoch microplate spectrophotometer.

The standard curve was plotted in Microsoft Excel and the concentrations of eluted protein samples were calculated by inserting the mean absorbance in the standard curve equation.

3.3 Lipid overlay assay

The binding of the recombinant GST-fusion proteins to different lipids were assessed by using PIP Strips™ overlay assay. Each pip strip consists of 100 pmol of different types of lipids spotted on a membrane. The assay was done under dark conditions. Each pip strip was placed in 5 mL blocking buffer (TBS, 1% (v/v) Tween-20, 3% (w/v) essential fatty acid free BSA), while gently shaking at RT for 1 hour. 2.5 µg GST-fused protein was added to the blocking buffer and left to incubate under the same conditions for 1 hour. Next, the lipid blots were washed six times in 5 mL TBS-T (TBS, 1% (v/v) Tween-20), while gently shaking at RT for 5 min. After washing, the lipid blots were incubated with anti-GST antibody conjugated to horse radish peroxidase (HRP) in 1:50000 dilution in blocking buffer. The membranes were left to incubate for 1 hour before being washed in TBS-T as previously described. Before exposing the lipid blots, SuperSignal™ West Pico PLUS Chemiluminescent Substrate was added on the membrane and incubated for 5 min. Blots were imaged using a ChemiDoc XRS+™ and ImageJ was used to quantify the chemiluminescent signal intensity in pixels.

3.4 Fluorescence Denaturation Assay

The stability of GST cleaved proteins were investigated in a thermal stability assay. Upon gradually increasing temperatures, the state of protein denaturation was measured by the Perkin-Elmer LS-50 Fluorescence Spectrometer. A blank measurement was performed at 10°C with the SEC elution buffer (50 mM Tris-HCl pH 8, 400 mM NaCl, 0.5 mM TCEP). The excitation was performed at 295 nm and the emission measurements were carried out in Hellma Quartz cuvettes, at 328 nm and 352 nm for the temperatures: 10, 15, 25, 30, 35, 40, 45, 50, 55, 60, 65, 70, 80, 90 and 95°C in water bath. The i328/i352 intensity ratios were calculated from the measurements. The Tm value (where denatured and native protein are in a 1:1 ratio) was found by fitting the temperature values against the i328/i352 in a Boltzman Sigmoidal function.

3.5 Cell Work

3.5.1 Cell maintenance

All work on living cells was done under sterile conditions. AU565 cell cultures were cultivated in RPMI-1640 medium, supplemented with 10% fetal bovine serum (FBS), and 1% penicillin streptomycin (PS), Growing cell cultures were kept in a humidified incubator at 37°C and 5% CO_2.

3.5.2 Cell Freezing

Cells growing in 10 cm petri dishes were lifted from the plate as described under cell splitting. Trypsin was carefully removed, the loosened cells were then resuspended in 5 mL RPMI-1640 (10% FBS, 1% PS) medium, centrifuged at 900 rpm, for 5 min and the supernatant discarded. The remaining cell pellet was resuspended in 1mL freezing medium (RPMI-1640 10% DMSO, 10 FBS, 1% PS) and transferred to a cryo tube, which were placed in a "Mr. Frosty", freezing container, in a -80°C freezer, ensuring the cells only decreased the temperature 1°C/min, before being moved to long time storage in liquid nitrogen tanks, at -150°C.

3.5.3 Cell thawing

AU565 cells were retrieved from storage in liquid nitrogen tanks and thawed quickly in a 37°C water bath. 6 mL RPMI-1640 (10% FBS, 1% PS) medium, preheated to 37°C, was used to resuspend the cells, before centrifugation at 900 rpm, for 5 min and discarding the supernatant. The pellet was resuspended in 10 mL medium and seeded on a 10 cm petri dish. The cells were left to recover, in the incubator, and ready to use at 75%-100% confluency.

3.5.6 Cell splitting

AU565 cells were split when they were between 75% - 100% confluent. Fcells were washed in sterile RT PBS. trypsin preheated to 37°C was added, and the cells placed in the incubator, at 37°C and 5% CO_2. When the cells could be observed loosening from the plate,

under the microscope, trypsin was removed. The cells were resuspended in 5 mL 37°C warm RPMI-1640 (10% FBS, 1% PS) before being split, no thinner than 1:5, in a new 10 cm dish. A total volume of 10 mL medium was mixed with the cells and placed in the incubator.

For transfection, cells were seeded on glass coverslips at 3.5 10^5 cells/well in 2 mL in 6-well plates.

3.5.7 Transfection

The medium was changed into 2 mL RPMI-1640 (10% FBS, no PS) per well, 2-3 hours before transfecting the cells with pEGFP constructs. The transfection was performed with Lipofectamine™ 3000 Transfection Reagent, where the plasmid to lipofectamine 3000 reagent ratio was 1:3. 125 µL RT Opti-MEM medium was mixed with 6 µL lipofectamine 3000 reagent. Another 125 µL RT optimum medium was mixed with 2 µg plasmid and 4 µL P3000 reagent. Both solutions were left to incubate at RT, for 5 min. The Lipofectamine solution was transferred into the tube with the DNA and P3000. The solution was mixed by gentle vortexing, left to complex at RT for 25 min and added dropwise to the cells. The cells were placed in the incubator O/N. A medium change was performed the morning after transfection, to 2 mL RPMI-1640 (20% FBS, no PS) and cells were placed back in the incubator to recover. 48 hours after addition of transfection complexes, the cells were ready to be fixed.

3.5.8. Immunostaining and microscopy

Cells transfected with pEGFP constructs were fixed, immunostained and mounted but protected from light, due to EGFP being light sensitive. Firstly, 2 mL PBS preheated to 37°C was used for washing the cells. Cell fixing was performed in 2 mL 3.7% paraformaldehyde (PFA) in PBS preheated to 37°C for 10 min, under the fume hood due to PFA toxicity. After washing 3x in 2 mL PBS, cell permeabilization was conducted by adding 1 mL permeabilization solution (0.25% Triton-X100 in 1x PBS) for 10 min at RT. The cells were then blocked in 1mL blocking buffer (3% free fatty acid BSA/goat serum, 0.05% Triton-X100 in 1xPBS) for 1 hour, at RT, and then incubated with 60 µL of 1:400 anti-Nucleolin (C13C) mAb Rabbit and 1:500 anti-Fibrillarin Rabbit (C13C3) mAb primary antibodies diluted in blocking buffer for 1 hour at RT in a humid chamber. The coverslips were washed 4x, for 5 min, at RT,

while shaking in wash buffer (0.1% Tween-20 in 1xPBS) before being incubated with secondary antibody Alexa Fluor™ 594 goat anti-mouse IgG (H+L) in 1:200 dilution in blocking buffer, for 1 hour at RT. The coverslips were again washed as described in the washing step above and mounted on glass slides on ProLong™ Glass Antifade Mountant with NucBlue™. The localization of EBP1 protein constructs were visualized by Leica epifluorescence microscope DMI 6000B.

4 Results

4.1 C-terminal mutations on EBP1 were introduced by PCR point mutation.

Our group previous study showed that EBP1 binds PPIn through a N-terminal and a C-terminal lysine rich binding domain (Figure 9 A) (Karlsson et al., 2016). During the study of the interaction of EBP1 with PPIn, the group encountered, through the cBioPortal and Catalogue Of Somatic Mutations In Cancer (Cosmic), several mutations located in the C-terminal motif of EBP1 in tumors (table 4.1.1). We focused on the following four mutations in this thesis, Q367H, Q367K, K373E-Ins and K372R-Del (Cerami et al., Cancer Discov. 2012, and Gao et al., Sci. Signal. 2013, (Tate et al., 2018). There have been some previous experiments on the K373E-Ins and K372R-Del in our group by previous master students, but the Q367H and Q367K mutants were introduced for the first time in this study. By continuing the work on EBP1 C-terminal mutants the aim is to understand the function of the C-terminal binding motif

Table 4.4.1. EBP1 C-terminal motif tumour mutants.
Data from Catalogue Of Somatic Mutation In Cancer v94 May 2021 ND: not determined

Mutation	Effect of mutation on aa sequence	Tumour samples	PPIn interaction	Nucleolar localisation
K372Rfs *16 (c1115del)	K372R + Change in aa composition post K372R	large intestine (5), pancreas (1), stomach (1), ovary (1)	increased	Highly retained
K373Efs*19 (c1115dup)	K373E + change in aa composition post K373E	large intestine (2), stomach (1)	ND	Highly retained

Q367K (c1099C>A)		Thyroid (4)	ND	ND
Q367H (c1101G>C)		urinary tract (1), upper aerodigestive tract (1)	ND	ND

The two newly introduced mutations Q367H and Q367K are both missense, point and substitution mutations where the glutamine 367 is changed to a new amino acid (Figure 9 B). In the Q367K mutant the neutrally charged glutamine is changed to a positively charged lysine, increasing the consecutive lysines in the motif from six to seven, possibly making the motif more reactive. The same glutamine was changed to another positive amino acid, histidine in the Q367H mutation. Since Q367H is very similar to the Q367K mutation it will likely have a similar effect. To investigate the effects of these mutations, both mutations were introduced into EBP1 WT by PCR in two different vectors (Figure 9 A); pEGFP-C2, a mammalian expression vector coding for the protein with an EGFP tag, and the pGEX-4T-2 vector, a bacterial expression vector fusing the protein to a GST-tag.

The K373E-Ins mutation is a frameshift mutation where a single nucleotide is inserted in the codon, coding for lysine 373, and exchanging this amino acid for glutamate (Figure 9 B). This shortens the C-terminal motif from six to five lysines, as well as creating a frameshift, causing the protein to shorten by 4 amino acids and changing the remaining amino acid composition to an overall more positive charge.

The K372R-Del mutation is another frameshift mutation (Figure 9 B), in this case a nucleotide is deleted, causing lysine K372R to be replaced by arginine, thus shortening the lysin motif from six to four lysins. The deletion creates a frameshift, which also changes, and increases the charge on the remaining amino acids. The mutated tail, codes for an early stop codon, shortening the tail by eight amino acids. With less lysines present and shorter C-terminal tail, effective binding of ligand might be hindered/reduced.

Previously in our group EBP1-K372R-Del had been cloned into the pEGPF-C2 and pGEX-4T-2 vectors (Figure 9 A). The K373E-Ins was previously cloned into the pEGFP-C2 vector, therefore in this study we introduced K373E-Ins in the pGEX vector as well (Figure 9 A). In addition, Q367H and Q367K were introduced in pGEX-4T2-EBP1 and pEGFP-C2. Cloning in these vectors will allow for protein expression with GST and EGFP tag allowing us

to study the effect of EBP1 mutations in various experiments, such as immunostaining on protein localization, PPIn binding and protein stability.

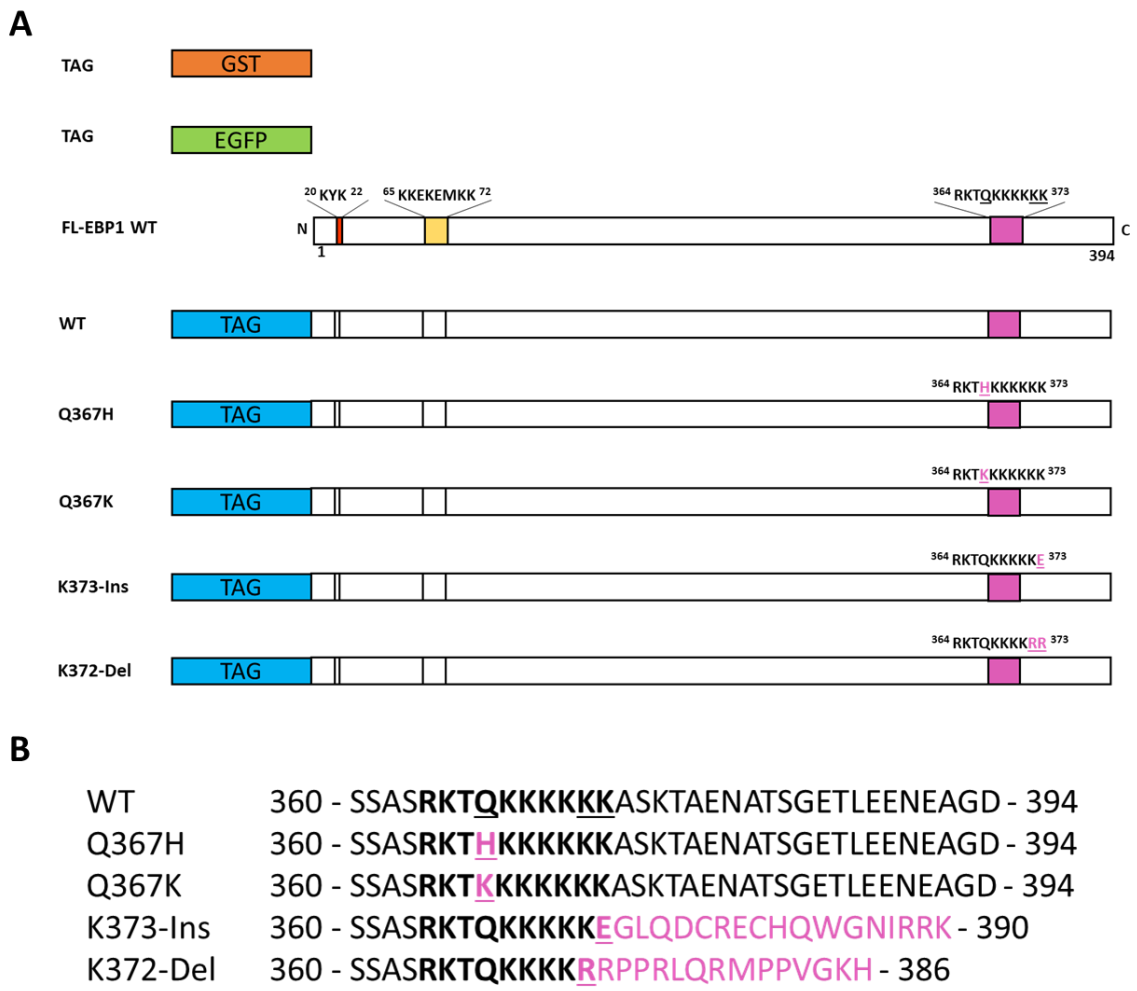

Figure 9. Schematic representation of EBP1 tumor mutants in the C-terminal binding motif.

A) EBP1 is a 394 amino acids protein with a nuclear localization signal (NLS) (red), a lysine rich N-terminal (yellow), and C-terminal (magenta) motif. Mutations in the C-terminal motif of EBP1 were created by PCR in pEGFP-C2 vector, causing the protein to be expressed with a EGFP tag (green), and in a pGEX-4T-2 vector combining expressed protein with a GST tag (orange). The picture is not to scale. B) Location and amino acid sequence of C-terminal motif mutations.

4.2 Expression and purification of GST fused EBP1 WT and tumor mutant proteins

pGEX-4T2-EBP1 construct were transformed in BL-21 Codon Plus (DE3)-RIL cells for protein expression and purification on Glutathione Sepharose beads. Aliquots from each purification step was collected and run on SDS-PAGE (Figure 10). Eluted GST-tagged protein was collected for pip-strip assay. The GST tag is 26 kDa and EBP1 is 48 kDa protein which combined generate a 72 kDa fusion protein. However, thrombin can cleave the GST-EBP1 fusion protein when GST is bound to the beads. EBP1 will then elute without the tag and can be run through SEC on ÄKTA. All the GST-EBP1 proteins showed a clear band on the SDS-PAGE located right below the 75 kDa marker, thus corresponding to GST-tagged EBP1. Each of the proteins; GST-EBP1-WT (Figure 10 A), GST-EBP1-Q367H (Figure 10 B), GST-EBP1-Q367K (Figure 10 C), GST-EBP1-K373E-Ins (Figure 10 D), and GST-EBP1-K372R-Del (Figure 10 E) followed the same expression and purification pattern. The band corresponding to GST-EBP1 fusion increased in thickness after induction with IPTG. After lysis of the induced cells, a lot of protein remained in the pellet, though an ample amount could be found in the supernatant as well. Noticeably after the GST binding process to Glutathione Sepharose beads the lysate, collected as the first flowthrough still held a thick GST-EBP1 band, indicating that a large number of the protein, does not bind to the beads. The lack of binding might be due to nonoptimal conditions or maybe too few beads present for binding. In the last flowthrough after several washes, most of the proteins had been removed, the sample was clear with only a few weak bands. The exception was GST-EBP1-K373E-Ins where the last flowthrough sample was completely clear of any protein bands.

The eluted protein samples show clear and strong GST-EBP1 bands as well as some impurities or degradation bands, showing the same pattern on the gel, but at different strengths. While GST-EBP1-WT (Figure 10 A), GST-EBP1-Q367H (Figure 10 B) and GST-EBP1-K372R-Del (Figure 10 E) showed the most impurities, a weaker impurities pattern was observed for GST-EBP1-Q367K (Figure 10 C), and GST-EBP1-K373E-Ins had the highest purity with less contaminating bands (Figure 10 D). Even though there were some contamination present, the proteins were pure enough and in high enough amount that they could be used in proteomics studies.

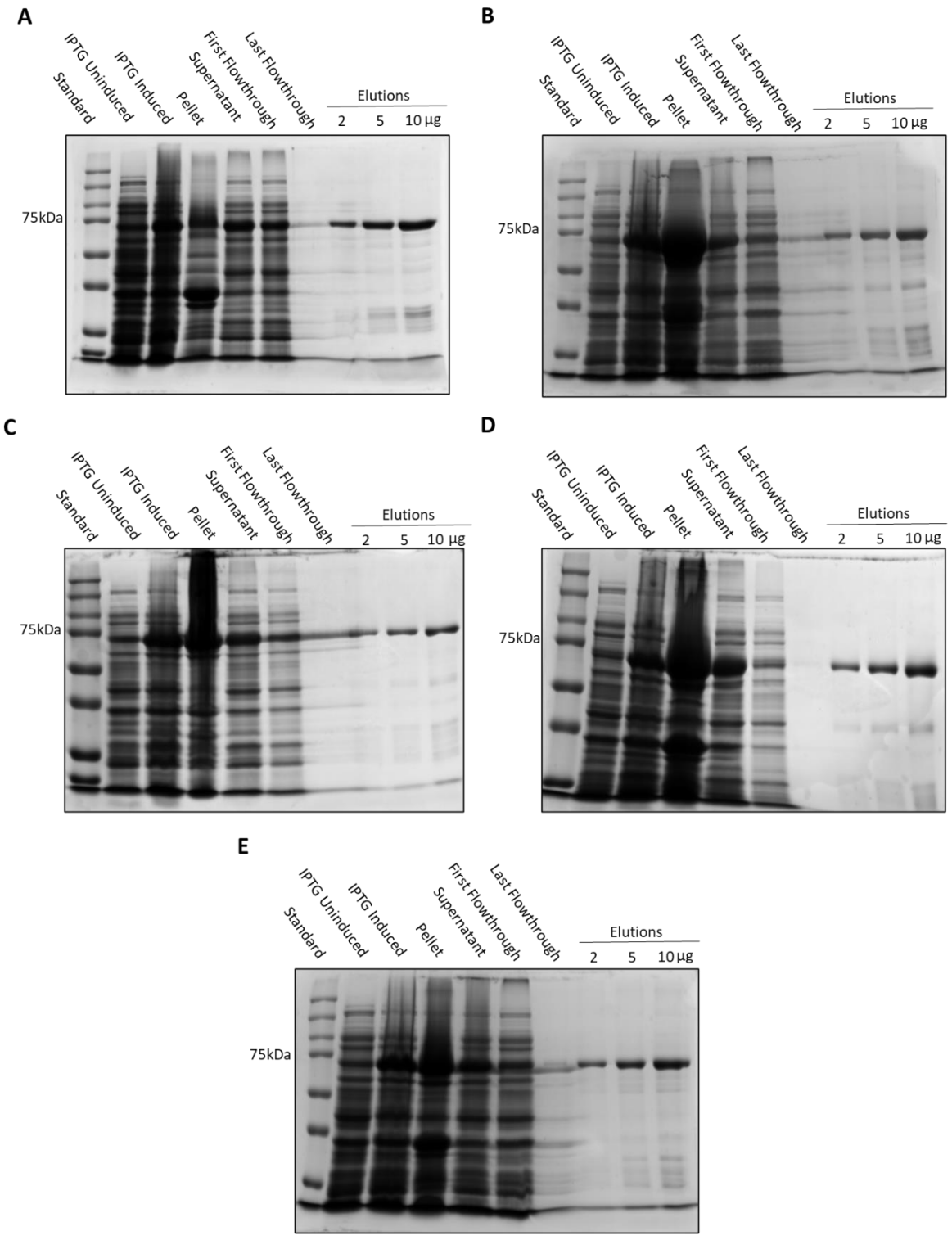

Figure 10 Expression and purification of GST-EBP1 constructs.
A) GST-EBP1-WT, B) GST-EBP1-Q367H, C) GST-EBP1-Q367K, D) GST-EBP1-K373E-Ins, and E) GST-EBP1-K372R-Del, were expressed in BL-21 Codon Plus (DE3)-RIL cells. Protein expression was induced with 0.5 mM Isopropyl β-D-thiogalactopyranoside (IPTG) for 3 h at 37°C while shaking at 250 rpm. After cell lysis, the lysate was centrifuged at 3200 g for 15 min. EBP1 was purified through binding lysate supernatant on Glutathione Sepharose beads. The protein concentration was obtained through Bradford colorimetric assay. From each purification

step, samples were collected and run on 10% SDS-PAGE, with Precision Plus Protein™ Dual Color Standards. The gels were stained with InstantBlue™ Coomassie staining, and pictures taken with Bio-Rad GelDoc™ EZ Imager.

4.3 Size Exclusion chromatography of GST-cleaved EBP1 proteins

GST tagged EBP1 wt/Q367K/K372R-Del were first purified trough affinity chromatography on glutathione Sepharose beads and the tag cleaved by thrombin, so it would be possible to work with only the protein. Cleaved proteins were purified by size exclusion chromatography (SEC) on ÄKTA with the program UNICORN, before using the protein in thermal denaturation assays. As the protein samples were purified on ÄKTA the UV detectors measured the absorbance at 280 nm, giving the UV- chromatograms for EBP1 WT (Figure 11 A), EBP1-372R-Del (Figure 11 B) and EBP1-Q367K (Figure 11 C). The chromatograms showed in which fractions the protein may have eluted in. By running the fractions of interest on SDS-PAGE, successful purification of the EBP1 proteins was confirmed (Figure 11 D).

The chromatogram for EBP1 wt (Figure 11 A) shows the protein purification profile for absorbance measured at 280 nm. The high peak after 46.73 mL (fractions A), is likely the void volume, where proteins too large for the pores would elute. However, when running a sample on SDS-PAGE (Figure 11 D) a faint EBP1 wt band was detected 50kDa, corresponding well to the expected 48kDa EBP1 size. After 55.46mL, a second peak appeared with an intensity of approximately 700mAU, where EBP1 was expected to elute (B Fractions). Corresponding fractions were pooled, the concentration acquired by NanoDrop1000 using extinction coefficients from Expasy ProtParam and subsequently run on SDS-PAGE (figure 11 D). On the control gel, a clear band, with increasing strength with the protein amount could be seen at ca. 50kDa, also some negligible protein impurities were present. The small sized salts eluted last, after 131.9 mL buffer ran through the column. In conclusion, EBP1 wt was successfully purified for further use. The purification profile for EBP1-K372R-Del (Figure 11 B) shows a peak after 46.45 mL (fraction A) for the void volume, no clear protein band could be detected (figure 11 D). After 56.02 mL a peak with an intensity of ca. 300mAU (fraction B) was detected. The protein concentration was determined, and samples were run on the SDS-PAGE (Figure 11 D) as described above. On the gel a single strong band at approximately

50kDa with increasing strength depending on increasing protein amount was visible. There were very little contaminants, making the ÄKTA purification successful. The UV-chromatogram for EBP1-Q367K (Figure 11 C) showed several peaks. The twofirst peaks eluted at 49.38mL and 55.32ml (fractions A) is the likely void volume. The fourth peak eluted after 83.85mL, contains other contaminants, smaller than EBP1, in this case likely thrombin. The large peak 106.90mL is where the salts elute. EBP1-Q367K is probably located in the eluted B fractions after 61.72mL. The fractions from the peak were run on the SDS-PAGE (Figure 11 D). The gels show single protein bands located at approximately 50kDa for all the fractions, including the expected void volume (fraction A), which might contain some aggregated protein. Some impurities, a few faint protein bands are also visible. The EBP1-Q367K was considered pure enough to proceed to thermal denaturation assay.

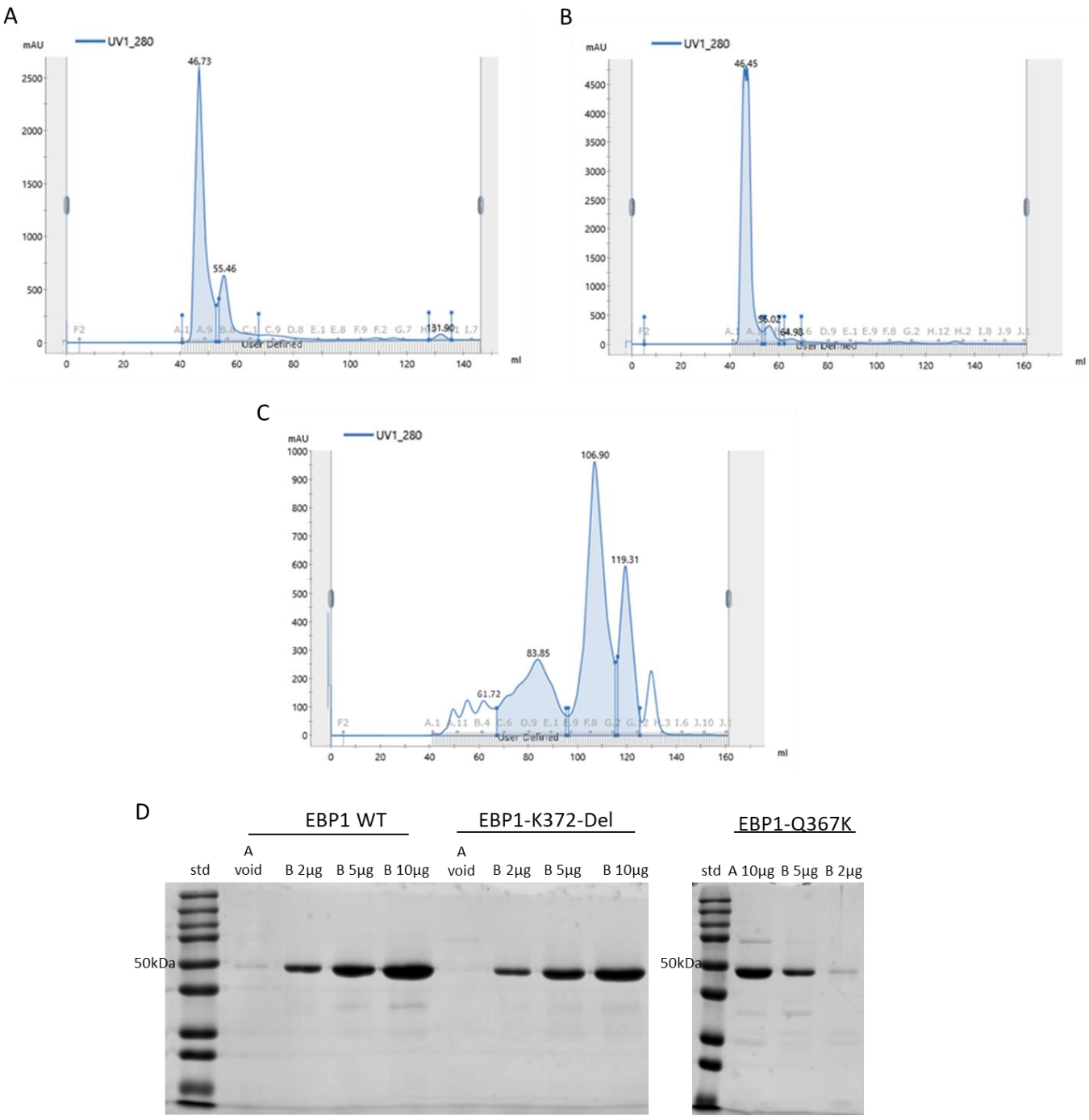

Figure 11. Size Exclusion chromatography of GST cleaved EBP1 proteins.
The GST-EBP1 wt/K372R-Del/Q367K constructs were expressed in BL21 Codon Plus (DE3)-RIL cells, purified on GST Sepharose beads and cleaved with Thrombin. After removal of GST tag a second purification on ÄKTA by SEC on Superdex 75 was carried out. A) UV Chromatogram of EBP1 wt, B) Chromatogram of EBP1-K372R-Del, C) Chromatogram of EBP1-Q367K, and D) protein fractions from A9 and B9 (WT and K372R-Del), and A10, B12 and B5 (Q367K) run on 10% SDS-PAGE and stained with InstantBlue™ Coomassie staining and imaged by Bio-Rad GelDoc™ EZ Imager.

4.4 C-terminal mutated EBP1 had increased PIP binding affinity on lipid blots

Through a PtdIns(4,5)P_2-pulldown assay of nuclear proteins, our group had first identified EBP1 as a binding partner for PtdIns(4,5)P_2. The lysine rich C-terminal motif (364-RKTQKKKKKK-373) was then characterized by use of lipid blot as an important PPIn binding motif for EBP1 (Karlsson et.al, 2016). Since EBP1 was established as a PPIn binding protein, it was relevant to investigate whether the mutations in the C-terminal binding domain would affect PIP binding.

After expression and purification of EBP1, the concentration was determined through Bradford assay. Pipstrips, membranes spotted with 15 different lipids were incubated with the recombinant proteins, GST-EBP1-WT, GST-EBP1-Q367H, GST-EBP1-Q367K, and GST-EBP1-K373E-Ins (Figure 12 A). PIP binding affinity was visualized by incubating the blots with anti-GST-HRP, and imaged with ChemiDoc XRS+™, the binding interaction was quatified using ImageJ.

The WT lipid blot exhibit binding to all PPIn, but strongest to the monophosphorylated, less binding for PtdIns(3,5)P_2, PtdIns(3,5)P_2, and PA, WT only bound weakly to PtdIns(3,4)P_2, PtdIns(3,4,5)P_3, and PS. Q367H and K373E-Ins exhibited similar PPIn binding pattern compared to the WT on the pip strip assay (Figure 12 A). The fold difference in signal intensity for the mutants compared to WT (Figure 12 B), affirm the PPIn binding was the same for Q367H and K373E-Ins. The fold difference was approximately 1 for the monophosphorylated and bisphosphorylated PPIn, the exception being PtdIns. Binding to PtdIns(3,4,5)P_3 and PA differed on the other hand and was increased by approximately two fold.

The Q367K mutant stood out (Figure 12 A), as it bound all the same PIPs as the wt, but overall binding was dramatically stronger. Q367K had increasing binding affinity to PPIn with increasing number of phosphate groups. The monophosphorylated PPIn had between one and twofold binding increase, bisphosphorylated PPIn increased from two to sixfold, the triphosphorylated PtdIns(3,4,5)P_3 increased most, with eightfold binding difference. In addition, increased binding was observed for PA and PS as well. Due to the increased PPIn

binding demonstrated by the Q367K mutant, the lipid overlay assay was repeated for WT and Q367K, with a new batch of expressed and purified protein (Figure 12 C). Both WT and Q367K match well with the trend in the original lipid blot. However, the binding intensity abated in the repeat. This bear true in the quantification as well (Figure 12 E). The binding trend, where binding affinity increased with the number of phosphate groups, was not present in the repeated blot. PtdIns(3,4,5)P_3 decreased drastically in the new blot, from eightfold to 1.5 fold, suggesting the reduced protein activity in the repeat

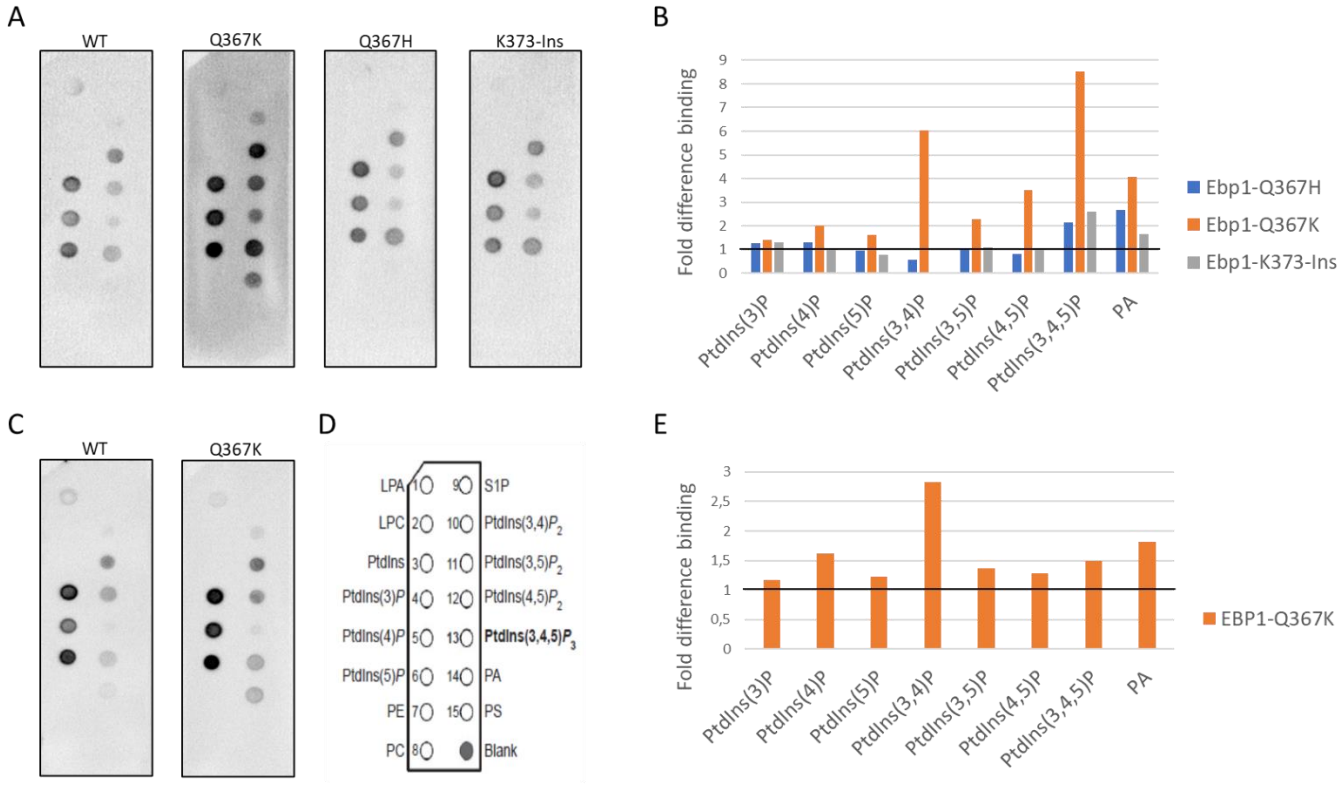

Figure 12. Binding of recombinant GST-EBP1 to PPIn.
Lipid blots (nitrocellulose membranes spotted with 100pmol phospholipids from Echelon Bioscience) were incubated with 0.5 µg/mL GST-EBP1-WT,Q367H,Q367K, or K373E-Ins. The blots were incubated with 1:50000 anti-GST antibody conjugated to horse radish peroxidase (HRP) and the signal intensity measured at 425 nm with (A) 1 sec and (C) 10 sec exposure imaged by ChemiDoc XRS+™. The Quantification of pixel intensity of each spot was done in ImageJ and the diagram in Excel. A) Lipid overlay assay of GST-EBP1-WT/Q367H/Q367K/K373E-Ins, B) Quantification of lipid blot A, as the fold difference in mutant EBP1 compared to WT EBP1 binding to each PPIn. C) Repeat lipid overlay assay of GST-EBP1-wt and GST-EBP1-Q367K. E) Quantification of pixel intensity for Q367K compared to WT. D) Map of the lipids spotted on nitrocellulose membrane. Lysophosphatic acid (LPA), Lysophosphocholine (LPC), Phosphatidylinositol (PtdIns), Phosphatidylinositol 3-phosphate (PtdIns3P), PtdIns4P, PtdIns5P, Phosphatidylethanolamine (PE), Phosphatidylcholine (PC),

Sphingosine-1-Phosphate (S1P), PtdIns(3,4)P_2, PtdIns(3,5)P_2, PtdIns(4,5)P_2, PtdIns(3,4,5)P_3, Phosphatic acid (PA), Phosphatidylserine (PS), and Blank.

4.5 The thermal stability of EBP1 remains unaffected by the Q367K and K372R-Del mutations

Initial fluorescence thermal stability assays were performed for EBP1 wt, and the two tumor mutants Q367K and K372R-Del. These two mutant proteins were chosen for the assay, due to their tendency in previously conducted experiments to affect protein functionality, at a higher magnitude compared to the other two mutants (Q367H and K373E-Ins). The purpose was to see if the mutations affected the protein stability.

The proteins purified by SEC (Figure 11) were used for the thermal stability assay. Gradually EBP1 proteins were heated between 10°C and 95°C. Every 5°C the samples were exited at 295 nm and the emission measured at 328 nm and 352 nm and the intensity ratio, i328/i352 was calculated. The temperature was plotted against i328/i352 ratio and fitted to a sigmoidal curve, giving the thermal denaturation curve for each of the EBP1 proteins (Figure 13). The inflexion point, where half of the proteins are in their native and the other half in the denatured/disorganized state were extracted, from the denaturation curve in the form of Tm values.

The thermal curve for EBP1 WT (Figure 13. A) had a nice shape, the ratio was scattered closely around a planar pretransition state starting at ca. 1.3 intensity and lasting from 10°C to 40°C degrees, between 45°C and 60°C the curve slope linearly downward, before ebbing into the planar post transition state, with 0.8 i328/i352. The inflexion point was located in the middle of the slope and the Tm for EBP1 was found to be 52°C. The curve obtained from EBP1-Q367K thermal denaturation (Figure 13 B) was similar in shape to the WT. In this case the pretransition state started with 1.08 i328/i352 ratio, downward slope from 40°C to 60°C and a posttransition state at ca. 0.74 i328/i352. The downward slope gave 51.6°C Tm value for EBP1-Q367K. EBP1-K372R-Del curve (Figure 13 C) had a pretransition state at 1.2 intensity ratio, and posttransition state from 60°C with intensity ratio of 0.8. The downward slope area was between 50°C and 60°C. EBP1-K372R-Del precipitated at the inflexion area between 50°C and 55°C, affecting the shape of the curve, causing the curve to

go down perpendicular, instead of a gentler slope. Despite the precipitation a Tm value of 50.2°C was gained from the curve for EBP1-K372R-Del.

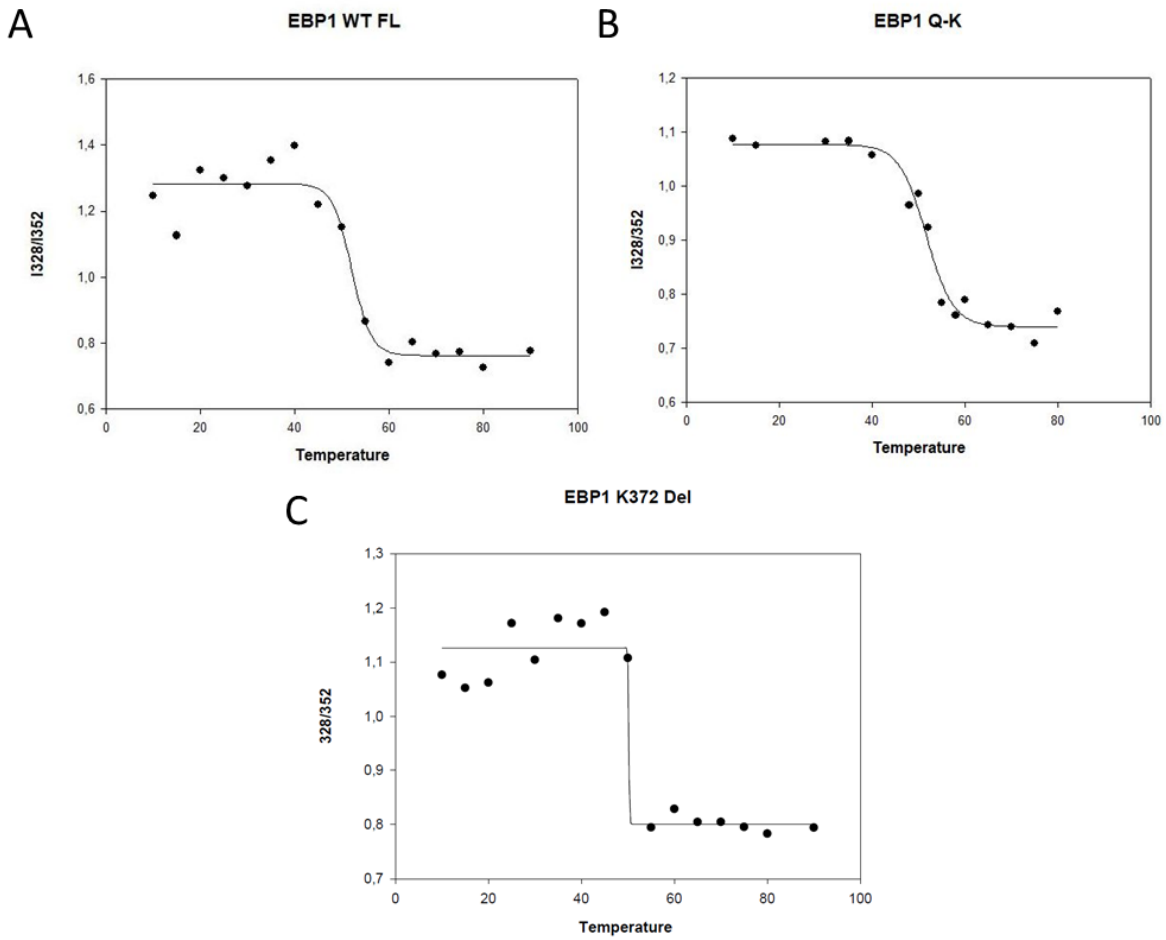

Figure 13. Thermal denaturation curve for EBP1 constructs.
EBP1-wt/Q367K/K372R-Del were prepared for denaturation assays by expression in BL21 Codon Plus (DE3)-RIL cells, purification, and cleavage of GST tag on Sepharose beads, followed by SEC. Upon gradually heating the protein samples between 10°C and 95°C degrees the samples were excited at 295 nm, and the emission at 328 nm and 352 nm was measured. The temperature was plotted against the intensity ratio, i328/i352 and fitted against a Boltzman Sigmoidal function, giving the denaturation curves and melting temperature (Tm) for A) EBP1 wt, B) EBP1-Q367K, and C) EBP1 -K372R-Del. N.B. EBP1-K372R-Del visibly precipitated causing a loss of points situated between 50°C and 55°C.

4.6 C-terminal mutations affect the localization of EBP1 in the cell

Previously, EBP1 was shown to localize in the nucleolus through the C-terminal amino acids 301-394 (Squatrito et al., 2004a). Later our group expanded on this knowledge realizing

the C-terminal motif 364-RKTQKKKKKK-373 was an important part of the region required for nucleolar localization (Karlsson et al., 2016). Our group also showed previously that the C-terminal binding motif contributed more to nucleolar localization when compared to the N-terminal motif (Karlsson et al., 2016). Since there already are examples where a substitution mutation, K372RN, in the motif, prevented nucleolar localization, as well as mutation of four lysines (K469-K372R) in another mutant prevented its localization in the nucleolus (Karlsson et al., 2016), it is reasonable to suspect this might be the case for other mutations. In this thesis it was of interest to figure out if the C-terminal mutations affects nucleolar localization. To do that AU565 cells were transfected with pEGFP-EBP1-WT, pEGFP-EBP1-Q367H, pEGFP-EBP1-Q367K, pEGFP-EBP1-K373E-Ins, and pEGFP-EBP1-K372R-Del and visualized by fluorescence microscopy.

EBP1 localized in three main patterns (Figure 14 A). The first pattern is a nucleolar pattern where EGFP-EBP1 was localized in cytoplasm and nucleoli. In the intermediate pattern EBP1 was found in the cytoplasm, and did not localize to the nucleoli, though it could be present at varying levels in the nucleus. The third pattern was a non-nucleolar pattern, with EBP1 localized in the cytoplasm and nucleus, but excluded from the nucleoli.

The occurrence of each pattern in cells transfected with the varying EBP1 constructs were quantified (Figure 14 B). From the quantification of the patterns, the same trend emerges for all proteins. The nucleolar pattern was the most common, emerging in more than 50% of the cells for all proteins. The intermediate pattern was also very common to see. Fewest observed cells had the non-nucleolar pattern. Representative images are shown in Figure 14 A.

The level of non-nucleolar cells increased for all four mutants compared to WT. In EBP1 K372R-Del had increased nucleolar level of 68% (Table 4.6.1), compared to WT, while the intermediate level was reduced to 29%. The WT however had 60% nucleolar and 39% intermediate localization in the cells. Just 1 % of WT transfected cells had non nucleolar pattern, however the number was 14% and 11% of Q367K and K373E-Ins transfected. Suggesting there might be a trend where the non-nucleolar pattern is more common for Q367K and K373E-Ins. The Q367H mutation behaved very similar to WT.

Our group had previous experience with K373E-Ins and K372R-Del, the number of nucleoli per cell increased compared to the WT. Hence, we decided to further investigate the effect of all the C-terminal mutations on nucleoli number, the number of EGFP-EBP1 positive nucleoli in each cell was counted and displayed in percentage (Figure 15 B). WT, Q367H and Q367K had approximately 40% cells without EGFP-EBP1 positive nucleoli (table 4.6.1 and figure 14 B). The K372R-Del mutant on the other hand, had only 32% zero EGFP-EBP1 positive nucleoli, showing a tendency toward higher number of nucleoli in the cells. The nucleolar pattern consists of one or more nucleoli in the cell. The overarching trend for all construct is, one nucleoli per cell, while increasing number of nucleoli appears with less frequency (Figure 15 B). WT and Q367H EBP1 displayed similar nucleolar trends, with 37% and 15% EBP1 WT having one or two nucleoli respectively, while in the case of EBP1 Q367H 44% and 13% had one or two nucleoli. 3% of Q367H and 8% WT had three or more nucleoli per cell. In the case of EBP1-Q367K mutant, the percentage of cells with one nucleolus was reduced to 29% , while 17% and 9% of the cells had 2 or 3 nucleoli. K373E-Ins and K372R-Del cells showed a higher percentage, 17% and 13% respectively, of cells with 3 or more nucleoli per cell, which indicate these two mutants may cause an increased number of nucleoli.

The immunostaining experiment also showed where the different EGFP-EBP1 constructs localize in the cell (Figure 15 A). The empty vector pEGFP-C1 was used as control, with EGFP localizing in the cytoplasm and nucleus. The WT EBP1 was restricted to the cytoplasm and nucleoli, the same can be seen for the Q367H. Q367K and K373E-Ins both exhibit a nucleolar pattern in some cells, while a non-nucleolar pattern can be observed in other cells. The K372R-Del showed three cells having nucleolar pattern, where one contained a higher number, five large nucleoli, also a non-nucleolar cell was present.

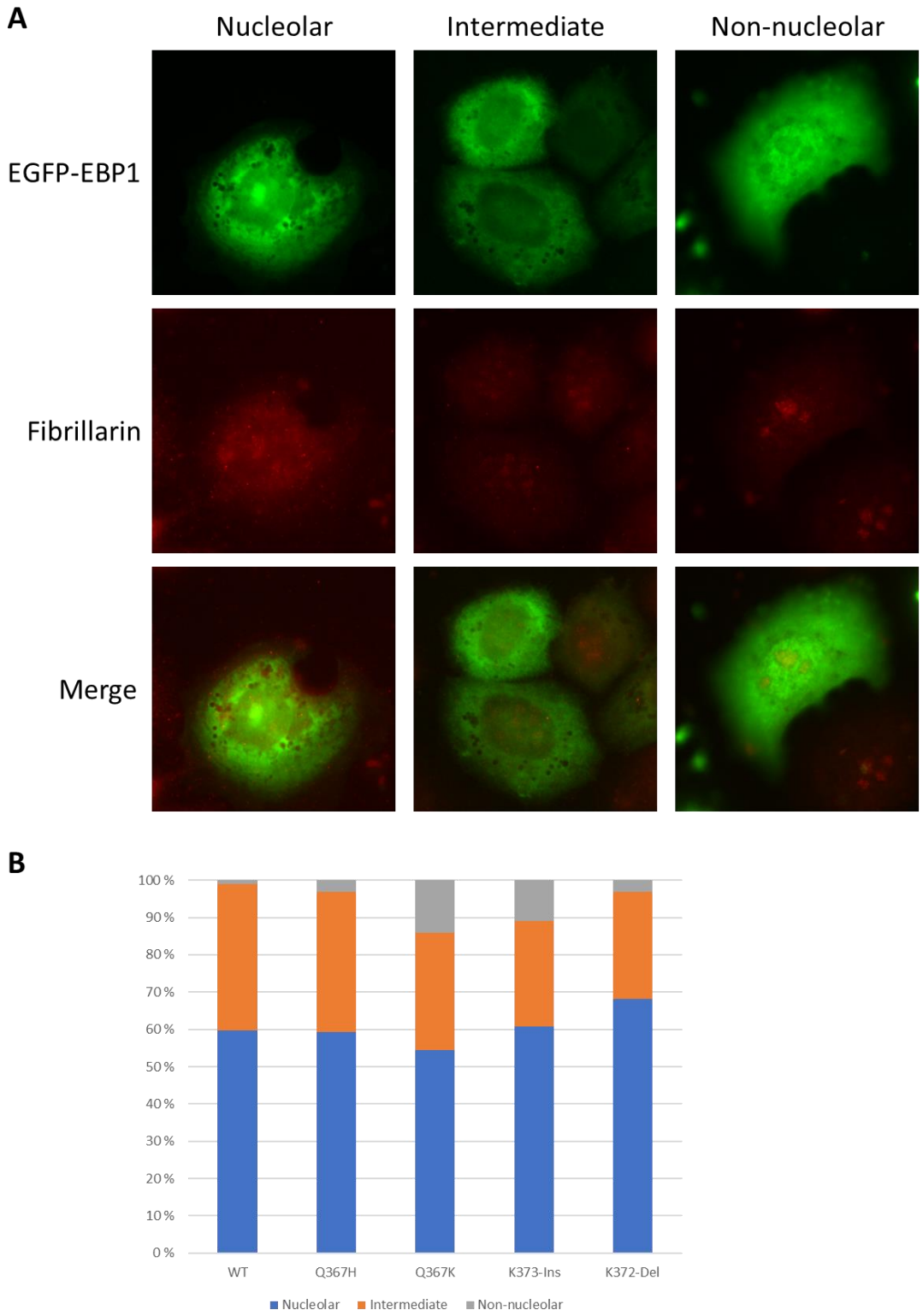

Figure 14. EGFP-EBP1 constructs localize in three main patterns in the cell.
AU565 cells were transfected with pEGFP-EBP1-WT/Q367H/Q367K/K373E-Ins/K372R-Del, immunostained with primary antibody, fibrillarin and secondary Alexa Fluor™ 594, and imagined with fluorescence microscopy. A) Example of the three main EGFP-EBP1 localization patterns are: Nucleolar, EBP1 locates in cytoplasm and nucleolus Intermediate, EBP1 locates in cytoplasm and various levels in the nucleus. Non-nucleolar, EBP1 locates in

cytoplasm and nucleus, but is excluded from nucleoli. B) Quantification in percentage of EGFP-EBP1 variant localization pattern, based on the number of cells for each protein: WT 92 cells, Q367H 32 cells, Q367K 58 cells, K373E-Ins 47 cells, K372R-Del 63 cells. state this is representative of 2 experiments but 1 was quantified.

Table 4.6.1. **Percentage of EBP1 construct localization.**

% EGFP-EBP1	WT	Q367H	Q367K	K373E-Ins	K372R-Del
Nucleolar	59,7826087	59,375	55,2	60,8695652	68,2539683
Intermediate	39,1304348	37,5	31,0344828	28,2608696	28,5714286
Non-nucleolar	1,08695652	3,125	13,7931034	10,8695652	3,17460317

A

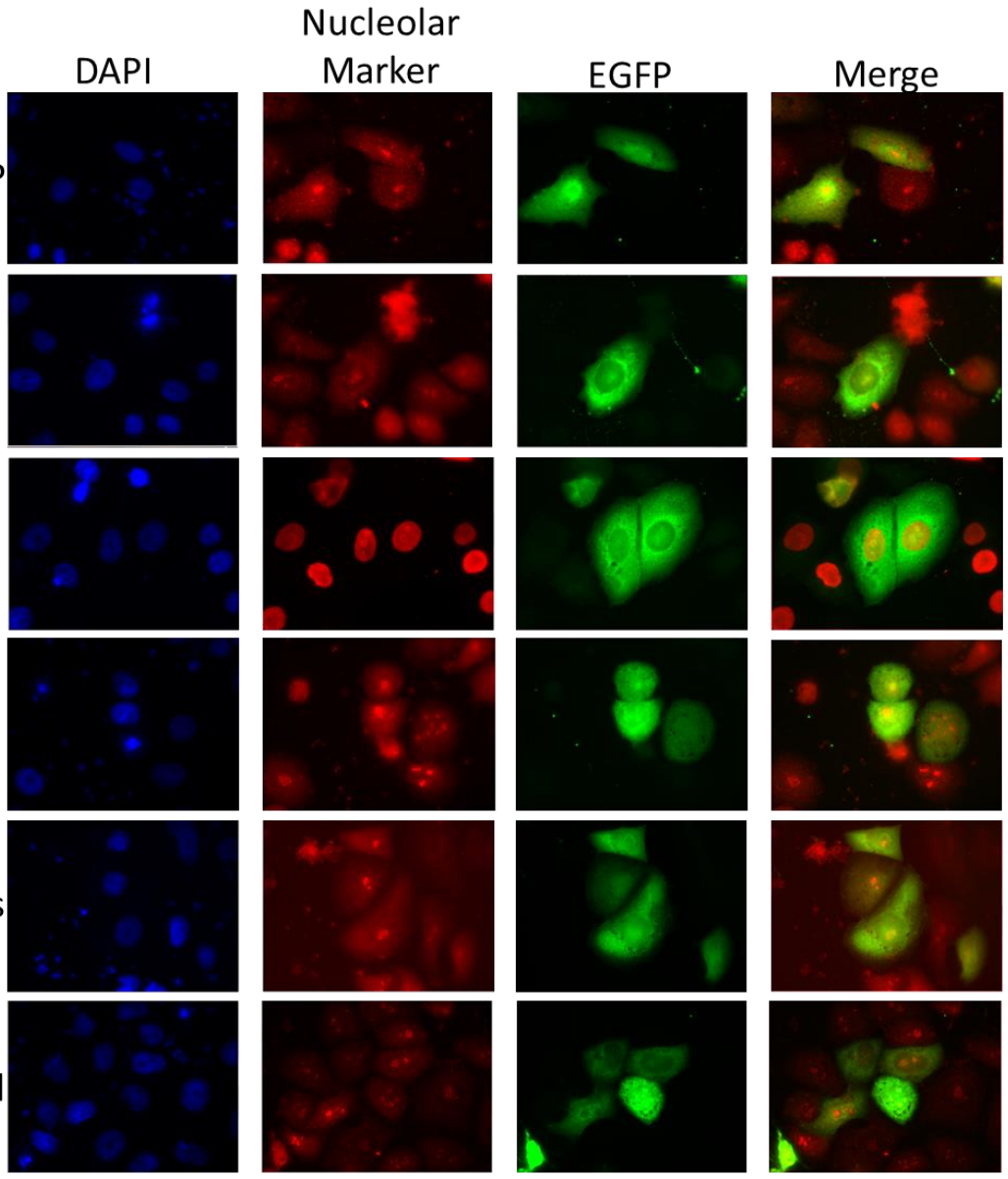
DAPI
Nucleolar Marker
EGFP
Merge
EGFP
WT
Q367H
Q367K
K373-Ins
K372-Del

B

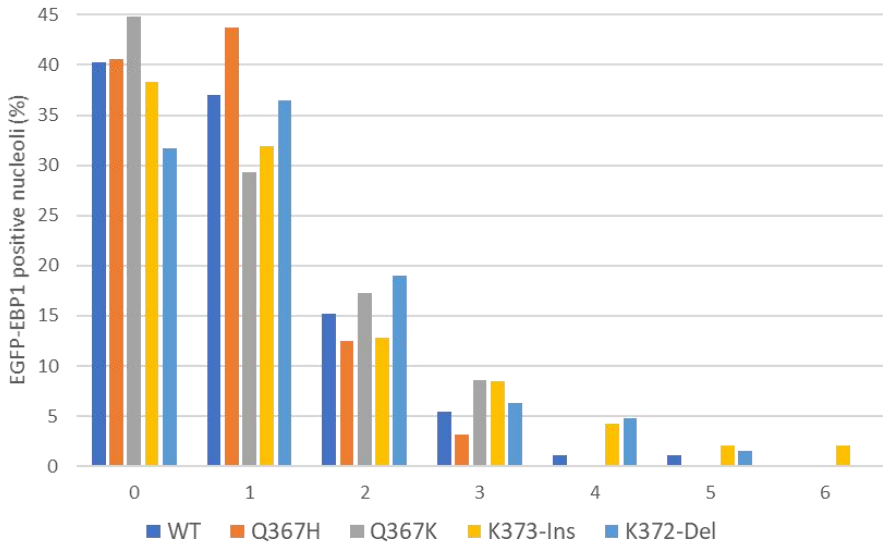
EGFP-EBP1 positive nucleoli (%)
45
40
35
30
25
20
15
10
5
0
0
1
2
3
4
5
6
WT
Q367H
Q367K
K373-Ins
K372-Del

Figure 15. EBP1 C-termini mutations affect localization nucleoli number.
A) Representative fluorescence microscopy pictures of AU565 cells transfected with pEGFP-EBP1-WT/Q367H/Q367K/K373E-Ins/K372R-Del and immunostained with the nucleolar marker fibrillarin, (except Q367H, where nucleolin was used) and secondary antibody Alexa Fluor™ 594, B) Percentwise quantification of EGFP-EBP1 positive nucleoli per cell, for each construct. The sample size for each construct was: 92 cells for WT, 32 cells for Q367H, 58 cells for Q367K, 47 cells for K373E-Ins, and 63 cells for K372R-Del.

Table 4.6.2. Percentage of nucleoli number per cell for each construct.

GFP positive nucleoli (%)	WT	Q367H	Q367K	K373E-Ins	K372R-Del
0	40,2	40,6	44,8	38,3	31,7
1	37,0	43,8	29,3	31,9	36,5
2	15,2	12,5	17,2	12,8	19,0
3	5,4	3,1	8,6	8,5	6,3
4	1,1	0,0	0,0	4,3	4,8
5	1,1	0,0	0,0	2,1	1,6
6	0,0	0,0	0,0	2,1	0,0

5 Discussion

The functional effect caused by mutations in EBP1. The mutations are located withing the C-terminal (PBR) of EBP1, were discovered in various cancer tissues. Q367H and Q367K are two missense mutations exchanging a neutral amino acid for a positively charged amino acids. Two frameshift mutations were studied as well, K373E-Ins and K372R-Del. Both frameshifts coded for an early stop codon and increased the positive charge on the remaining protein. The PBR had previously been shown to have dual function, containing a nucleolar localization sequence overlapping with a lysine rich binding motif (364-RKTQKKKKKK-373), which also contained the mutations of interest. Q367K, K373E-Ins and K372-Del were revealed to likely influence nucleolar localization of EBP1 in an immunostaining localization experiment. The mutational effect on EBP1 binding ability was investigated through a PIP strip assay, indicating a possible loss of specificity and increased binding of negatively charged PPIn by the Q367K mutation. Lastly preliminary testing of EBP1 stability in a thermal denaturation assay showed the mutations likely did not influence protein stability.

5.1 EBP1 localization

PtdIns(4,5)P_2, has previously been identified as a nuclear signaling lipid (add refs). EBP1 was identified as a possible binding protein, interacting with PtdIn(4,5)P_2, through nuclear protein pull down assays and quantitative mass spectrometry (Lewis et al., 2011). EBP1 binding ability was confirmed through a pip strip assay where recombinant EBP1 bound to several PPIn, in addition to PtdIn(4,5)P_2 (Karlsson et al., 2016). Many proteins bind PPIn through pleckstrin homology (PH), Phox-homology (PX) and Fab1, YOyoTB, Vac1, EE A1 (FYVE) domains facilitating binding through headgroup binding, membrane insertion and electrostatic interactions (Lemmon, 2008). EBP1 however does not contain any of these domains, instead binding is enabled through electrostatic interactions of the polybasic region (PBR), a region characterized by basic amino acids . EBP1 was shown to harbor two PBRs located N-terminal and a C-terminal of the protein (add ref Karlsson et al, 2016Within the C-terminal PBR, a lysine rich binding motif (364-RKTQKKKKKK-373) has been described following the characteristic of a KR motif K/R-($X_{n=3-7}$)-KXKK (Lewis et al., 2011; Martin, 1998). In particular, four lysines, K369-K372R) were shown to be necessary for PPIn binding (add ref Karlsson et al, 2016). In addition, a putative nucleolar localization sequence (NoLS) was obtained for aa 357-385, overlapping with the C-terminal binding motif (Karlsson et al., 2016). The study from Karlsson *et al* showed the requirement for these four lysines for the localization of EBP1 in the nucleolus. The overlapping binding motif and NoLS suggest dual function of the EBP1 PBR domain, localization and binding. Several C-terminal mutations on EBP1; Q367H, Q367K, K373E-Ins and K372R-Del have been discovered in various cancer tissues (Cerami et al., Cancer Discov. 2012, and Gao et al., Sci. Signal. 2013, (Tate et al., 2018). This study strived to learn how the mutations affect EBP1 functionality.

Several studies have given an indication that C-terminal mutations alter functionality. One study created an EBP1 mutant cutting the C-terminal (from Q367), located within the C-terminal motif, causing EBP1 to be unable to localize in the nucleoli, instead it existed mainly in the nucleoplasm and cytoplasm (Squatrito et al., 2004b). Another study, performed by our group on a different tumor mutant K372RN, resulted in an intermediate pattern, where EBP1 localized in the cytoplasm and nucleus, but not in nucleoli (Karlsson et al., 2016). The four C-terminal mutations investigated in this study are also located within the same lysine rich

motif, prompting the obvious question, how localization will be influenced by the mutations?

The Q367H EBP1 mutant exhibited a similar localization pattern to the WT, and most EGFP-EBP1 localized in nucleolar pattern and the remaining in intermediate. Similarities were represented in the number of nucleoli as well. The similar pattern trend and number of nucleoli between WT and Q367H, indicate that the Q367H mutation does not influence EBP1 localization in the cell. Interestingly the Q376H mutation is the only one of the four in this study, which does not change any lysins in the C-terminal motif, which may lead to the belief, nucleolar localization is either mainly or exclusively regulated by the consecutive lysins in the motif.

Cells transfected with the Q367K EBP1 mutant showed a slight decrease in nucleolar localization and a high number of non-nucleolar cells. One speculate the possibility that EBP1 localization for Q367K is not static, but that it transitions from diffuse nucleolar localization to either the nucleolar or non-nucleolar pattern.

The K372R-Del mutation was the only mutant that showed a stronger preference for nucleolar localization more so than the other protein variants or the WT. The localization of this mutant was studied before and the results presented here show the same trend. However, the previous work showed somewhat a higher proportion of cells with nucleolar localization and with larger number of nucleoli in the cells at a much higher frequency.

K373E-Ins seems to exhibit acquire a pattern with characteristics of both the Q367K and K373E-Del mutation displayed a similar tendency to Q367K to avoid localization in nucleoli. On the other hand, a pattern reminding of K372R-Del was exhibited. A large percentage of the cells (60%) showed EGFP-EBP1 localize in nucleoli, half of which, 30% all the cells contained three or more nucleoli. Indicating the K373E-Ins mutation cause the cell to create more nucleoli, which is a location for cell cycle control (add a ref this is an important statement), which in turn might be how the mutation is a contributing factor the cancer development. The reason for increased number of nucleoli in K372R-Del and K373E-Ins is suspected to be the shorter more positive C-terminal tail. Strengthening EBP1 affinity for PPIn binding, thus increasing the likelihood/chance for nucleolar aggregation and localization.

5.2 PPIn binding

PtdIns(3,4,5)P_3 are lipids found to colocalize interact with EBP1 in the nucleoli (Karlsson et al., 2016) . Seeing as the C-terminal binding motif is mainly responsible for PPIn interactions, it was of interest to know in what way mutations in the motif may influence binding interaction. The endometrial tumor mutant K372RN, showed reduced PtdIns(3,4,5)P_3 binding (Karlsson et al., 2016), attesting that mutations in the C-terminal motif affect protein lipid interactions. Considering the reduced PPIn interaction for the K372RN mutation, it is likely that other mutations in the same motif also will influence EBP1 binding affinity. EBP1 WT, Q367H, Q367K, and K373E-Ins were produced with a GST tag for the purpose of testing the PPIn interaction on pipstrip assay. Binding interactions were quantified and fold binding difference calculated compared to WT. The WT bound to all the PPIn, mostly to monophosphorylated PPIn, less for bisphosphorylated and PA, and least for PtdIns(3,4,5)P_3. This was consistent with previous studies in our group (add Karlsson et al). Q367H and K373E-Ins showed similar binding pattern to WT, suggesting the mutations did not affect binding interaction. On the first lipid overlay assay, Q367K showed a large increase in binding to polyphosphorylated PPIn and PA. The largest binding increase however was for PtdIn(3,4,5)P_3, another nucleolar signaling lipid. This would be reasonable to observe due to the nature of the mutation. Likely the phosphate group position of the inositol ring causes specific binding. Q367K mutation is a missense mutation, which leaves the protein structure as is, except for expanding the C-terminal binding motif with a seventh lysine. The binding motif is arguably a KR motif, whose functionality is based upon repeated occurrences of the positively charged amino acids residues lysine and arginine (Lewis et al., 2011). It can be speculated that the addition of an extra lysine increases the positive charges in the binding motif, causing binding without recognizing specificity. The increased binding combined with lack of specificity may be a mechanism for which Q367K mutation contribute to the lack of signal regulation in cancer development. The C-terminal mutations binds to many proteins, especially the truncating ones change the sequence dramatically and would affect interaction.

The fold difference revealed that only PtdIn(3,4)P2, and PA had noticeably more EBP1 binding. The trend where EBP1 binding of more negatively charged phosphate groups was not present. Q367K exhibited two markedly different binding interactions on the two pip strip assays. All the same proteins were bound, but with less intensity on the repeat blot. Which assay is the more accurate cannot be deduced at the present, the experiment would have to be repeated.

5.3 EBP1 stability

Studies regarding stability are hard to come by. Therefore, a preliminary thermal denaturation assay of several EBP1 constructs were executed, to obtain thermodynamic data in the form of Tm, where 50% of the protein is denatured and 50% in native state. This was a limited assay, due to time constraints, only EBP1 WT and the Q367K and K372R-Del were assayed. Q367K and K372R-Del were prioritized for the experiment, because of their tendency in previous experiments to diverge from WT, such as Q367K have increased binding on pip strip assays and K372R-Del a tendency to induce increased number of nucleoli. These two were therefore believed more likely to veer from the WT stability.

The Tms given were 52.0°C for WT, 51.6°C for Q367K, and 50.2°C for K372R-Del. The Tm values were all very similar, indicating the mutations does not influence protein stability. EBP1 being unaffected by the mutations might be explained by the N-terminal. Due to the p42 isoform existing at lower levels in cancer cells compared to p48, it has been suggested that EBP1 stability is dependent on the N-terminal tail, particularly the first 48 N-terminal amino acids missing in p42 (Hwang et al., 2020). If it is the case that the N-terminal plays a dominant part in EBP1 stabilization, this might be an explanation for why the C-terminal mutations seems not to affect stability.

However, the K372R-Del mutant had a near 2°C lower Tm compared to WT, and lower Tm indicates less stable protein. In addition, it was observed that EBP1-K372R-Del visibly precipitated causing a loss of measurements at 50°C and 55°C. A possible reason for K372R-Del precipitation might be the shorter positively charged tail, perhaps altering protein interactions with the environment. Precipitation is usually caused by changed hydrophobicity and pH, causing the protein to aggregate and possible denature in the solution (Polson et al., 2003). Lower Tm value along with protein precipitation, suggest K372R-Del mutation on EBP1 might impact and reduce protein stability.

The idea of N-terminal control of protein stability has been strengthened by what is known about the structure of EBP1. The crystal structure of EBP1 was only partially solved(Kowalinski, Bange, Wild, et al., 2007; Monie et al., 2007). EBP1 likely have an unstructured C-terminal, having caused difficulties when crystallizing to deduce the structure. When producing the crystal, the largest obtained fragment was between amino acids 8-360. The 7 first and 34 last amino acids were not included in this structure (Monie et al., 2007). That include the lysine rich C-terminal binding motif. The floppy state of EBP1 was further corroborated by our group in PONDR, showing that the C-terminal was predicted to be highly disorganized (unpublished data). The notion of N-terminal importance for stability combined with the C-terminal already existing as an unstructured part of the protein, might explain why mutational effect on stability is minimal. The mutation is located in C-terminal which already was unstructured.

Even though the Tm values gained in this study are useful knowledge, the thermal denaturation assay is far from done. Recently strives forward have been made as a full EBP1 structure have been solved through CRYO EM in complex with ribosome subunit 80S (Bhaskar et al., 2021). In this case the C-terminal binding motif is involved in binding to the ribosomal subunit, stabilizing it to a point where the structure could be made out. This raises the question if EBP1 binding activity to ligand raises the protein stability. It is therefore of interest to perform several more denaturation assays, to deduce whether PPIn binding increases the stability for the WT, but also if ligand binding increases the stability for mutants compared to the wt. Increased stability in the thermal denaturation assay suggest increased binding activity, which might be an explanation for how the mutations contribute to cancer oncogenic development.

5.4 Concluding remarks and further perspective

Overall, we learned valuable knowledge of how the C-terminal binding motif behaves. Through immunostaining localization assays we validated the importance of NoLS in the C-terminal motif. Deduced from the Q367K, K373E-Ins and K372R-Del mutations show a tendency in immunostainings to affect localization. Moreover, due to the Q367H mutation being the only mutation in the C-terminal binding motif not causing a change in the six

consecutive lysines, as well as not affecting localization pattern, we suggest that the nucleolar localization of EBP1 is heavily dependent on the six consecutive lysins found in the motif. Further localization studies must follow, for the purpose of quantifying more cells to obtain more reliable numbers. In addition, we also noticed that K372R-Del behaved differently from previous experience in our group. K372R-Del behaved in a weaker fashion than normal, where it would be expected to see a lot more nucleolar pattern, in addition to increased number of nucleoli in the cells. Furthermore, it might be of interest to attempt to investigate the localization of EBP1 within the nucleoli in more details though electron microscopy. In addition, by detecting known EBP1 interacting biomolecules, such as PIP2, PIP3 and it might be possible to confirm colocalization and interaction through electron microscopy.

The mutations caused the positive charges in the C-terminal binding motif to increase, it would therefore be expected to see increased binding with negatively charged lipids on the pipstrip. Surprisingly Q367H and K373E-Ins revealed a binding pattern similar to WT, indicating the mutations did not affect binding. The Q367K mutation initially appeared to increase binding affinity for PPIn, when the negative charge increased. We surmise that increased binding affinity is caused by the mutation expanding the lysine rich motif, but otherwise retaining the protein structure/conformation. And it being the enlarged motif causing increased non-discriminating binding to PPIn. Nevertheless a repeat pipstrip assay was performed for Q367K which showed overall little changes to the WT. We don't know which blot is more representative, for this reason the experiment should be repeated. EBP1 should be re-expressed to evaluate the variation occurring between protein batches.

The thermal denaturation assay investigating protein stability for WT, Q367K and K372R-Del, was only a preliminary assay, due to time constraints. The assay gave similar Tm values for the protein variants, indicating the stability was unaffected by the mutations, possibly due to the C-terminal motif already being unstructured. Nevertheless the K372R-Del mutation showed some indication of different behavior. K372R-Del visibly precipitated after SEC purification, which led to loss of measurements, and a slightly lower Tm value, suggesting the mutation result in loss of stability. The thermal denatarution assay needs to be continued to further the structural understanding of EBP1 and its mutant. We would prefer

to repeat the experiment in triplicates for all EBP1 variants as well as investigating the experiment when EBP1 is bound to PPIn. We suspect that ligand binding stabilizes the C-terminal. A possible way the mutations may disrupt signal pathways and contribute to cancer development, is by either stably binding ligand for an extended period, or opposite, less stable binding, causing less EBP1 interaction and less signal. Thermal denaturation assay may reveal if any of the mutations cause EBP1 to affect binding in such a way.

Overall, the Q367H mutation behaved similar to WT during the experimentation, we don't learn much of how this function in cancer development. The lack of altered behavior in Q367H was surprising, since the Q367H and Q367K are so alike. Both mutations exchange a neutral glutamine for a new positively charged amino acid. The Q367H was not tested for in the thermal denaturation assay, possibly this would reveal something, about how it functions. However, it is likely that it will continue to behave as the WT, yet if bound to ligand perhaps this will drastically affect stability.

In addition, it would be advantageous to produce stable AU565 cell lines transfected with EGFP-EBP1 constructs. Stable cell lines would make it substantially easier to study EBP1 wt and mutant behavior in the cells, removing the need to constantly transfect the cells. Colony formation assay, where the EBP1 variants cell proliferation ability would be tested is an experiment that would be simplified by a stable cell lines.

6 References

Ball, L. A., & Kaesberg, P. (1973). Cleavage of the N-terminal formymlethionine residue from a bacteriophage coat protein in vitro. *Journal of Molecular Biology*, *79*(3), 531-537. https://doi.org/https://doi.org/10.1016/0022-2836(73)90404-X

Balla, T. (2013). Phosphoinositides: Tiny Lipids With Giant Impact on Cell Regulation. *Physiological Reviews*, *93*(3), 1019-1137. https://doi.org/10.1152/physrev.00028.2012

Bhaskar, V., Desogus, J., Graff-Meyer, A., Schenk, A. D., Cavadini, S., & Chao, J. A. (2021). Dynamic association of human Ebp1 with the ribosome. *Rna*, *27*(4), 411-419. https://doi.org/10.1261/rna.077602.120

Birbrair, A., Zhang, T., Wang, Z.-M., Messi, M. L., Enikolopov, G. N., Mintz, A., & Delbono, O. (2013). Role of pericytes in skeletal muscle regeneration and fat accumulation. *Stem cells and development*, *22*(16), 2298-2314. https://doi.org/10.1089/scd.2012.0647

Blunsom, N. J., & Cockcroft, S. (2020). Phosphatidylinositol synthesis at the endoplasmic reticulum. *Biochimica et Biophysica Acta (BBA) - Molecular and Cell Biology of Lipids*, *1865*(1), 158471. https://doi.org/https://doi.org/10.1016/j.bbalip.2019.05.015

Boronenkov, I. V., Loijens, J. C., Umeda, M., & Anderson, R. A. (1998). Phosphoinositide Signaling Pathways in Nuclei Are Associated with Nuclear Speckles Containing Pre-mRNA Processing Factors. *Molecular biology of the cell*, *9*(12), 3547-3560. https://doi.org/10.1091/mbc.9.12.3547

Bose, Sudeep K., Sengupta, Tapas K., Bandyopadhyay, S., & Spicer, Eleanor K. (2006). Identification of Ebp1 as a component of cytoplasmic bcl-2 mRNP (messenger ribonucleoprotein particle) complexes. *Biochemical Journal*, *396*(1), 99-107. https://doi.org/10.1042/BJ20051548

Colón-González, F., & Kazanietz, M. G. (2006). C1 domains exposed: From diacylglycerol binding to protein–protein interactions. *Biochimica et Biophysica Acta (BBA) - Molecular and Cell Biology of Lipids*, *1761*(8), 827-837. https://doi.org/https://doi.org/10.1016/j.bbalip.2006.05.001

Cui, D., Xiong, X., Shu, J., Dai, X., Sun, Y., & Zhao, Y. (2020). FBXW7 Confers Radiation Survival by Targeting p53 for Degradation. *Cell Reports*, *30*(2), 497-509.e494. https://doi.org/https://doi.org/10.1016/j.celrep.2019.12.032

De Craene, J.-O., Bertazzi, D. L., Bär, S., & Friant, S. (2017). Phosphoinositides, Major Actors in Membrane Trafficking and Lipid Signaling Pathways. *International Journal of Molecular Sciences*, *18*(3). https://doi.org/10.3390/ijms18030634

Figeac, N., Serralbo, O., Marcelle, C., & Zammit, P. S. (2014). ErbB3 binding protein-1 (Ebp1) controls proliferation and myogenic differentiation of muscle stem cells. *Developmental Biology*, *386*(1), 135-151. https://doi.org/https://doi.org/10.1016/j.ydbio.2013.11.017

Fujii, K., Susanto, T. T., Saurabh, S., & Barna, M. (2018). Decoding the Function of Expansion Segments in Ribosomes. *Mol Cell*, *72*(6), 1013-1020.e1016. https://doi.org/10.1016/j.molcel.2018.11.023

Gannon, P. O., Koumakpayi, I. H., Le Page, C., Karakiewicz, P. I., Mes-Masson, A.-M., & Saad, F. (2008). Ebp1 expression in benign and malignant prostate. *Cancer Cell International*, *8*(1), 18. https://doi.org/10.1186/1475-2867-8-18

Ganot, P., Jády, B. E., Bortolin, M. L., Darzacq, X., & Kiss, T. (1999). Nucleolar factors direct the 2'-O-ribose methylation and pseudouridylation of U6 spliceosomal RNA. *Mol Cell Biol*, *19*(10), 6906-6917. https://doi.org/10.1128/mcb.19.10.6906

Garcia, P., Gupta, R., Shah, S., Morris, A. J., Rudge, S. A., Scarlata, S., Petrova, V., McLaughlin, S., & Rebecchi, M. J. (1995). The pleckstrin homology domain of phospholipase C-.delta.1 binds with high affinity to phosphatidylinositol 4,5-bisphosphate in bilayer membranes. *Biochemistry*, *34*(49), 16228-16234. https://doi.org/10.1021/bi00049a039

Gilbert Di, P., & De Camilli, P. (2006). Phosphoinositides in cell regulation and membrane dynamics. *Nature*, *443*(7112), 651-657. https://doi.org/http://dx.doi.org/10.1038/nature05185

Goldman, R., Ben Levy, R., Peles, E., & Yarden, Y. (1990). Heterodimerization of the erbB-1 and erbB-2 receptors in human breast carcinoma cells: a mechanism for receptor transregulation. *Biochemistry*, *29*(50), 11024-11028. https://doi.org/10.1021/bi00502a002

Hammond, G. R. V., & Balla, T. (2015). Polyphosphoinositide binding domains: Key to inositol lipid biology. *Biochimica et Biophysica Acta (BBA) - Molecular and Cell Biology of Lipids*, *1851*(6), 746-758. https://doi.org/https://doi.org/10.1016/j.bbalip.2015.02.013

Hanahan, D., & Weinberg, R. A. (2000). The hallmarks of cancer. *Cell*, *100*(1), 57-70. https://doi.org/10.1016/s0092-8674(00)81683-9

Hernandez-Verdun, D. (2011). Assembly and disassembly of the nucleolus during the cell cycle. *Nucleus*, *2*(3), 189-194. https://doi.org/10.4161/nucl.2.3.16246

Hokin, L. E., & Hokin, M. R. (1955). Effects of acetylcholine on the turnover of phosphoryl units in individual phospholipids of pancreas slices and brain cortex slices. *Biochimica et Biophysica Acta*, *18*, 102-110. https://doi.org/https://doi.org/10.1016/0006-3002(55)90013-5

Hu, Y., Zhixue, L., & Ye, K. (2005). Phosphoinositol Lipids Bind to Phosphatidylinositol 3 (PI3)-Kinase Enhancer GTPase and Mediate Its Stimulatory Effect on PI3-Kinase and Akt Signalings. *Proceedings of the National Academy of Sciences of the United States of America*, *102*(46), 16853-16858. http://www.jstor.org/stable/4152310

https://www.ncbi.nlm.nih.gov/pmc/articles/PMC1283830/pdf/pnas-0507365102.pdf

Hwang, I., Ko, H. R., & Jee-Yin, A. (2020). The roles of multifunctional protein ErbB3 binding protein 1 (EBP1) isoforms from development to disease. *Experimental & Molecular Medicine*, *52*(7), 1039-1047. https://doi.org/http://dx.doi.org/10.1038/s12276-020-0476-z

Im, H., & Ham, S. (2020). Effect of linker on the binding free energy of stapled p53/HDM2 complex. *PLoS One*, *15*(4). https://doi.org/http://dx.doi.org/10.1371/journal.pone.0232613

Jacobsen, R. G., Mazloumi Gavgani, F., Edson, A. J., Goris, M., Altankhuyag, A., & Lewis, A. E. (2019). Polyphosphoinositides in the nucleus: Roadmap of their effectors and mechanisms of interaction. *Adv Biol Regul*, *72*, 7-21. https://doi.org/10.1016/j.jbior.2019.04.001

Jee-Yin, A., Liu, X., Liu, Z., Pereira, L., Cheng, D., Peng, J., Wade, P. A., Hamburger, A. W., & Ye, K. (2006). Nuclear Akt associates with PKC-phosphorylated Ebp1, preventing DNA fragmentation by inhibition of caspase-activated DNase. *EMBO Journal*, *25*(10), 2083-2095. https://doi.org/http://dx.doi.org/10.1038/sj.emboj.7601111

Jee-Yin, A., Rong, R., Liu, X., & Ye, K. (2004). PIKE/nuclear PI 3-kinase signaling mediates the antiapoptotic actions of NGF in the nucleus. *EMBO Journal*, *23*(20), 3995-4006. https://doi.org/http://dx.doi.org/10.1038/sj.emboj.7600392

Karlsson, T., Altankhuyag, A., Dobrovolska, O., Turcu, D. C., & Lewis, A. E. (2016). A polybasic motif in ErbB3-binding protein 1 (EBP1) has key functions in nucleolar localization and polyphosphoinositide interaction. *Biochem J*, *473*(14), 2033-2047. https://doi.org/10.1042/bcj20160274

Kawamura, K., Sato, N., Fukuda, J., Kodama, H., Kumagai, J., Tanikawa, H., Shimizu, Y., & Tanaka, T. (2003). Survivin acts as an antiapoptotic factor during the development of mouse preimplantation embryos. *Developmental Biology*, *256*(2), 331-341. https://doi.org/https://doi.org/10.1016/S0012-1606(02)00135-5

Kim, C. K., Lee, S. B., Nguyen, T. L. X., Lee, K.-H., Um, S. H., Kim, J., & Ahn, J.-Y. (2012). Long isoform of ErbB3 binding protein, p48, mediates protein kinase B/Akt-dependent HDM2 stabilization and nuclear localization. *Experimental Cell Research*, *318*(2), 136-143. https://doi.org/https://doi.org/10.1016/j.yexcr.2011.08.013

Kim, C. K., Nguyen, T. L. X., Joo, K. M., Nam, D.-H., Park, J., Lee, K.-H., Cho, S.-W., & Ahn, J.-Y. (2010). Negative Regulation of p53 by the Long Isoform of ErbB3 Binding Protein Ebp1 in Brain Tumors. *Cancer Research*, *70*(23), 9730. https://doi.org/10.1158/0008-5472.CAN-10-1882

Kim, H. H., Sierke, S. L., & Koland, J. G. (1994). Epidermal growth factor-dependent association of phosphatidylinositol 3-kinase with the erbB3 gene product. *Journal of Biological Chemistry*, *269*(40), 24747-24755. https://doi.org/https://doi.org/10.1016/S0021-9258(17)31455-2

Ko, H. R., Hwang, I., Jin, E.-J., Yun, T., Ryu, D., Kang, J.-S., Park, K. W., Shin, J.-H., Cho, S.-W., Lee, K.-H., Ye, K., & Ahn, J.-Y. (2019). Roles of ErbB3-binding protein 1 (EBP1) in embryonic development and gene-silencing control. *Proceedings of the National Academy of Sciences*, *116*(49), 24852. https://doi.org/10.1073/pnas.1916306116

Ko, H. R., Kim, C. K., Lee, S. B., Song, J., Lee, K. h., Kim, K. K., Park, K. W., Cho, S. w., & Ahn, J. y. (2014). P42 Ebp1 regulates the proteasomal degradation of the p85 regulatory subunit of PI3K by recruiting a chaperone-E3 ligase complex HSP70/CHIP. *Cell Death and Disease*, *5*, 12. https://doi.org/http://dx.doi.org/10.1038/cddis.2014.79

Koach, J., Holien, J. K., Massudi, H., Carter, D. R., Ciampa, O. C., Herath, M., Lim, T., Seneviratne, J. A., Milazzo, G., Murray, J. E., McCarroll, J. A., Liu, B., Mayoh, C., Keenan, B., Stevenson, B. W., Gorman, M. A., Bell, J. L., Doughty, L., Hüttelmaier, S., Oberthuer, A., Fischer, M., Gifford, A. J., Liu, T., Zhang, X., Zhu, S., Gustafson, W. C., Haber, M., Norris, M. D., Fletcher, J. I., Perini, G., Parker, M. W., Cheung, B. B., & Marshall, G. M. (2019). Drugging MYCN Oncogenic Signaling through the MYCN-PA2G4 Binding Interface. *Cancer Research*, *79*(21), 5652. https://doi.org/10.1158/0008-5472.CAN-19-1112

Kowalinski, E., Bange, G., Bradatsch, B., Hurt, E., Wild, K., & Sinning, I. (2007). The crystal structure of Ebp1 reveals a methionine aminopeptidase fold as binding platform for multiple interactions. *FEBS Letters*, *581*(23), 4450-4454. https://doi.org/https://doi.org/10.1016/j.febslet.2007.08.024

Kowalinski, E., Bange, G., Wild, K., & Sinning, I. (2007). Expression, purification, crystallization and preliminary crystallographic analysis of the proliferation-associated protein Ebp1. *Acta Crystallographica Section F*, *63*(9), 768-770. https://doi.org/doi:10.1107/S1744309107038985

Kramer, G., Rauch, T., Rist, W., Vorderwülbecke, S., Patzelt, H., Schulze-Specking, A., Ban, N., Deuerling, E., & Bukau, B. (2002). L23 protein functions as a chaperone docking site on the ribosome. *Nature*, *419*, 171-174. https://doi.org/10.1038/nature01047

Lamartine, J., Seri, M., Cinti, R., Heitzmann, F., & et al. (1997). Molecular cloning and mapping of a human cDNA (PA2G4) that encodes a protein highly homologous to the mouse cell cycle protein p38-2G4. *Cytogenetics and Cell Genetics*, *78*(1), 31-35. https://www.proquest.com/scholarly-journals/molecular-cloning-mapping-human-cdna-pa2g4-that/docview/224243289/se-2?accountid=8579

http://openurl.bibsys.no/openurl?url_ver=Z39.88-2004&rft_val_fmt=info:ofi/fmt:kev:mtx:journal&genre=article&sid=ProQ:ProQ%3Ahealthcompleteshell&atitle=Molecular+cloning+and+mapping+of+a+human+cDNA+%28PA2G4%29+that+encodes+a+protein+highly+homologous+to+the+mouse+cell+cycle+protein+p38-2G4&title=Cytogenetics+and+Cell+Genetics&issn=03010171&date=1997-01-01&volume=78&issue=1&spage=31&au=Lamartine%2C+J%3BSeri%2C+M%3BCinti%2C+R%3BHeitzmann%2C+F%3Bet+al&isbn=&jtitle=Cytogenetics+and+Cell+Genetics&btitle=&rft_id=info:eric/98005911&rft_id=info:doi/

Lee, S. B., Nguyen, T. L. X., Choi, J. W., Lee, K.-H., Cho, S.-W., Liu, Z., Ye, K., Bae, S. S., & Ahn, J.-Y. (2008). Nuclear Akt Interacts with B23/NPM and Protects It from Proteolytic Cleavage, Enhancing Cell Survival. *Proceedings of the National Academy of Sciences of the United States of America*, *105*(43), 16584-16589. http://www.jstor.org/stable/25465138

https://www.pnas.org/content/pnas/105/43/16584.full.pdf

Lemmon, M. A. (2008). Membrane recognition by phospholipid-binding domains. *Nature Reviews. Molecular Cell Biology*, *9*(2), 99-111. https://doi.org/http://dx.doi.org/10.1038/nrm2328

Lessor, T. J., & Hamburger, A. W. (2001). Regulation of the ErbB3 binding protein Ebp1 by Protein Kinase C. *Molecular and Cellular Endocrinology*, *175*(1), 185-191. https://doi.org/https://doi.org/10.1016/S0303-7207(01)00387-2

Lessor, T. J., Yoo, J.-Y., Xia, X., Woodford, N., & Hamburger, A. W. (2000). Ectopic expression of the ErbB-3 binding protein Ebp1 inhibits growth and induces differentiation of human breast cancer cell lines. *Journal of Cellular Physiology*, *183*(3), 321-329. https://doi.org/https://doi.org/10.1002/(SICI)1097-4652(200006)183:3<321::AID-JCP4>3.0.CO;2-O

Lewis, A. E., Sommer, L., Arntzen, M. O., Strahm, Y., Morrice, N. A., Divecha, N., & D'Santos, C. S. (2011). Identification of nuclear phosphatidylinositol 4,5-bisphosphate-interacting proteins by neomycin extraction. *Mol Cell Proteomics*, *10*(2), M110 003376. https://doi.org/10.1074/mcp.M110.003376

Liu, L., Li, X. D., Chen, H. Y., Cui, J. S., & Xu, D. Y. (2015). Significance of Ebp1 and p53 protein expression in cervical cancer. *Genet Mol Res*, *14*(4), 11860-11866. https://doi.org/10.4238/2015.October.2.19

Liu, Z., Ahn, J.-Y., Liu, X., & Ye, K. (2006). Ebp1 isoforms distinctively regulate cell survival and differentiation. *Proceedings of the National Academy of Sciences of the United States of America*, *103*(29), 10917-10922. https://doi.org/10.1073/pnas.0602923103

Liu, Z., Oh, S.-M., Okada, M., Liu, X., Cheng, D., Peng, J., Brat, D. J., Sun, S.-y., Zhou, W., Gu, W., & Ye, K. (2009). Human BRE1 is an E3 ubiquitin ligase for Ebp1 tumor suppressor. *Molecular biology of the cell*, *20*(3), 757-768. https://doi.org/10.1091/mbc.e08-09-0983

López, D. J., Rodríguez, J. A., & Bañuelos, S. (2020). Nucleophosmin, a multifunctional nucleolar organizer with a role in DNA repair. *Biochimica et Biophysica Acta (BBA) - Proteins and Proteomics*, *1868*(12), 140532. https://doi.org/https://doi.org/10.1016/j.bbapap.2020.140532

Martin, T. F. J. (1998). Phosphoinositide lipids as signaling molecules: Common themes for signal transduction, cytoskeletal regulation, and membrane trafficking. *Annual Review of Cell and Developmental Biology*, *14*, 231. https://www.proquest.com/scholarly-journals/phosphoinositide-lipids-as-signaling-molecules/docview/217974017/se-2?accountid=8579

http://openurl.bibsys.no/openurl?url_ver=Z39.88-2004&rft_val_fmt=info:ofi/fmt:kev:mtx:journal&genre=article&sid=ProQ:ProQ%3Ahealthcompleteshell&atitle=Phosphoinositide+lipids+as+signaling+molecules%3A+Common+themes+for+signal+transduction%2C+cytoskeletal+regulation%2C+and+membrane+trafficking&title=Annual+Review+of+Cell+and+Developmental+Biology&issn=10810706&date=1998-01-01&volume=14&issue=&spage=231&au=Martin%2C+T+F+J&isbn=&jtitle=Annual+Review+of+Cell+and+Developmental+Biology&btitle=&rft_id=info:eric/&rft_id=info:doi/

https://www.annualreviews.org/doi/10.1146/annurev.cellbio.14.1.231?url_ver=Z39.88-2003&rfr_id=ori%3Arid%3Acrossref.org&rfr_dat=cr_pub%3Dpubmed

McCrea, H. J., & De Camilli, P. (2009). Mutations in Phosphoinositide Metabolizing Enzymes and Human Disease. *Physiology*, *24*(1), 8-16. https://doi.org/10.1152/physiol.00035.2008

Monie, T. P., Perrin, A. J., Birtley, J. R., Sweeney, T. R., Karakasiliotis, I., Chaudhry, Y., Roberts, L. O., Matthews, S., Goodfellow, I. G., & Curry, S. (2007). Structural insights into the transcriptional and translational roles of Ebp1. *EMBO Journal*, *26*(17), 3936-3944. https://doi.org/http://dx.doi.org/10.1038/sj.emboj.7601817

Neilson, K. M., Abbruzzesse, G., Kenyon, K., Bartolo, V., Krohn, P., Alfandari, D., & Moody, S. A. (2017). Pa2G4 is a novel Six1 co-factor that is required for neural crest and otic development. *Developmental Biology*, *421*(2), 171-182. https://doi.org/https://doi.org/10.1016/j.ydbio.2016.11.021

Nevins, J. R. (2001). The Rb/E2F pathway and cancer. *Hum Mol Genet*, *10*(7), 699-703. https://doi.org/10.1093/hmg/10.7.699

Nguyen, L. X. T., Zhu, L., Lee, Y., Ta, L., & Mitchell, B. S. (2016). Expression and Role of the ErbB3-Binding Protein 1 in Acute Myelogenous Leukemic Cells. *Clinical Cancer Research*, *22*(13), 3320. https://doi.org/10.1158/1078-0432.CCR-15-2282

Ou, K., Kesuma, D., Ganesan, K., Yu, K., Soon, S. Y., Lee, S. Y., Goh, X. P., Hooi, M., Chen, W., Jikuya, H., Ichikawa, T., Kuyama, H., Matsuo, E.-i., Nishimura, O., & Tan, P. (2006). Quantitative Profiling of Drug-Associated Proteomic Alterations by Combined 2-Nitrobenzenesulfenyl Chloride (NBS) Isotope Labeling and 2DE/MS Identification. *Journal of Proteome Research*, *5*(9), 2194-2206. https://doi.org/10.1021/pr060115n

Payrastre, B., Missy, K., Giuriato, S., Bodin, S., Plantavid, M., & Gratacap, M.-P. (2001). Phosphoinositides : key players in cell signalling, in time and space. *Cellular Signalling*, *13*(6), 377-387. https://doi.org/https://doi.org/10.1016/S0898-6568(01)00158-9

Pederson, T. (1998). The plurifunctional nucleolus. *Nucleic Acids Research*, *26*(17), 3871-3876. https://doi.org/10.1093/nar/26.17.3871

Politz, J. C. R., Hogan, E. M., & Pederson, T. (2009). MicroRNAs with a nucleolar location. *RNA (New York, N.Y.)*, *15*(9), 1705-1715. https://doi.org/10.1261/rna.1470409

Polson, C., Sarkar, P., Incledon, B., Raguvaran, V., & Grant, R. (2003). Optimization of protein precipitation based upon effectiveness of protein removal and ionization effect in liquid chromatography–tandem mass spectrometry. *Journal of Chromatography B*, *785*(2), 263-275. https://doi.org/https://doi.org/10.1016/S1570-0232(02)00914-5

Radomski, N., & Jost, E. (1995). Molecular Cloning of a Murine cDNA Encoding a Novel Protein, p38-2G4, Which Varies with the Cell Cycle. *Experimental Cell Research*, *220*(2), 434-445. https://doi.org/https://doi.org/10.1006/excr.1995.1335

Raghu, P., Joseph, A., Krishnan, H., Singh, P., & Saha, S. (2019). Phosphoinositides: Regulators of Nervous System Function in Health and Disease [Review]. *Frontiers in Molecular Neuroscience*, *12*(208). https://doi.org/10.3389/fnmol.2019.00208

Raška, I., Shaw, P. J., & Cmarko, D. (2006). Structure and function of the nucleolus in the spotlight. *Current Opinion in Cell Biology*, *18*(3), 325-334. https://doi.org/https://doi.org/10.1016/j.ceb.2006.04.008

Reyes-Gutierrez, P., Ritland Politz, J. C., & Pederson, T. (2014). A mRNA and Cognate MicroRNAs Localize in the Nucleolus. *Nucleus*, *5*(6), 636-642. https://doi.org/10.4161/19491034.2014.990864

Roussel, P., André, C., Comai, L., & Hernandez-Verdun, D. (1996). The rDNA transcription machinery is assembled during mitosis in active NORs and absent in inactive NORs. *Journal of Cell Biology*, *133*(2), 235-246. https://doi.org/10.1083/jcb.133.2.235

Shah, Z. H., Jones, D. R., Sommer, L., Foulger, R., Bultsma, Y., D'Santos, C., & Divecha, N. (2013). Nuclear phosphoinositides and their impact on nuclear functions [https://doi.org/10.1111/febs.12543]. *The FEBS Journal*, *280*(24), 6295-6310. https://doi.org/https://doi.org/10.1111/febs.12543

Shaw, P., & Brown, J. (2012). Nucleoli: Composition, Function, and Dynamics. *Plant Physiology*, *158*(1), 44-51. http://www.jstor.org/stable/41435441

https://www.ncbi.nlm.nih.gov/pmc/articles/PMC3252080/pdf/44.pdf

Shaw, P. J., Highett, M. I., Beven, A. F., & Jordan, E. G. (1995). The nucleolar architecture of polymerase I transcription and processing. *The EMBO journal*, *14*(12), 2896-2906. https://www.ncbi.nlm.nih.gov/pmc/articles/PMC398408/pdf/emboj00036-0218.pdf

Sobol, M., Yildirim, S., Philimonenko, V. V., Marášek, P., Castaño, E., & Hozák, P. (2013). UBF complexes with phosphatidylinositol 4,5-bisphosphate in nucleolar organizer regions regardless of ongoing RNA polymerase I activity. *Nucleus*, *4*(6), 478-486. https://doi.org/10.4161/nucl.27154

Somanath, P., Bush, K. M., & Knoepfler, P. S. (2018). ERBB3-Binding Protein 1 (EBP1) Is a Novel Developmental Pluripotency-Associated-4 (DPPA4) Cofactor in Human Pluripotent Cells. *STEM CELLS*, *36*(5), 671-682. https://doi.org/https://doi.org/10.1002/stem.2776

Squatrito, M., Mancino, M., Donzelli, M., Areces, L., & Draetta, G. (2004a). EBP1 is a nucleolar growth-regulating protein that is part of pre-ribosomal ribonucleoprotein complexes. *Oncogene*, *23*, 4454-4465. https://doi.org/10.1038/sj.onc.1207579

Squatrito, M., Mancino, M., Donzelli, M., Areces, L. B., & Draetta, G. F. (2004b). EBP1 is a nucleolar growth-regulating protein that is part of pre-ribosomal ribonucleoprotein complexes. *Oncogene*, *23*(25), 4454-4465. https://doi.org/10.1038/sj.onc.1207579

Squatrito, M., Mancino, M., Sala, L., & Draetta, G. F. (2006). Ebp1 is a dsRNA-binding protein associated with ribosomes that modulates eIF2alpha phosphorylation. *Biochem Biophys Res Commun*, *344*(3), 859-868. https://doi.org/10.1016/j.bbrc.2006.03.205

Stevenson, B. W., Gorman, M. A., Koach, J., Cheung, B. B., Marshall, G. M., Parker, M. W., & Holien, J. K. (2020). A structural view of PA2G4 isoforms with opposing functions in cancer. *J Biol Chem*, *295*(47), 16100-16112. https://doi.org/10.1074/jbc.REV120.014293

Tate, J. G., Bamford, S., Jubb, H. C., Sondka, Z., Beare, D. M., Bindal, N., Boutselakis, H., Cole, C. G., Creatore, C., Dawson, E., Fish, P., Harsha, B., Hathaway, C., Jupe, S. C., Kok, C. Y., Noble, K., Ponting, L., Ramshaw, C. C., Rye, C. E., Speedy, H. E., Stefancsik, R., Thompson, S. L., Wang, S., Ward, S., Campbell, P. J., & Forbes, S. A. (2018). COSMIC: the Catalogue Of Somatic Mutations In Cancer. *Nucleic Acids Research*, *47*(D1), D941-D947. https://doi.org/10.1093/nar/gky1015

Taylor, A. (1993). Aminopeptidases: structure and function. *Faseb j*, *7*(2), 290-298. https://doi.org/10.1096/fasebj.7.2.8440407

Tsui, M. M., & York, J. D. (2010). Roles of inositol phosphates and inositol pyrophosphates in development, cell signaling and nuclear processes. *Advances in Enzyme Regulation*, *50*(1), 324-337. https://doi.org/https://doi.org/10.1016/j.advenzreg.2009.12.002

Viaud, J., Mansour, R., Antkowiak, A., Mujalli, A., Valet, C., Chicanne, G., Xuereb, J.-M., Terrisse, A.-D., Séverin, S., Gratacap, M.-P., Gaits-Iacovoni, F., & Payrastre, B. (2016). Phosphoinositides: Important lipids in the coordination of cell dynamics. *Biochimie*, *125*, 250-258. https://doi.org/https://doi.org/10.1016/j.biochi.2015.09.005

Wang, Y., Zhang, P., Wang, Y., Zhan, P., Liu, C., Mao, J.-H., & Wei, G. (2017). Distinct Interactions of EBP1 Isoforms with FBXW7 Elicits Different Functions in Cancer. *Cancer Research*, *77*(8), 1983. https://doi.org/10.1158/0008-5472.CAN-16-2246

Wild, K., Aleksić, M., Lapouge, K., Juaire, K. D., Flemming, D., Pfeffer, S., & Sinning, I. (2020). MetAP-like Ebp1 occupies the human ribosomal tunnel exit and recruits flexible rRNA expansion segments. *Nature Communications*, *11*(1). https://doi.org/http://dx.doi.org/10.1038/s41467-020-14603-7

Xia, X., Cheng, A., Lessor, T., Zhang, Y., & Hamburger, A. W. (2001). Ebp1, an ErbB-3 binding protein, interacts with Rb and affects Rb transcriptional regulation [https://doi.org/10.1002/jcp.1075]. *Journal of Cellular Physiology*, *187*(2), 209-217. https://doi.org/https://doi.org/10.1002/jcp.1075

Yan, G., & Ziff, E. (1995). NGF regulates the PC12 cell cycle machinery through specific inhibition of the Cdk kinases and induction of cyclin D1. *The Journal of Neuroscience*, *15*(9), 6200-6212. https://doi.org/10.1523/jneurosci.15-09-06200.1995

Yildirim, S., Castano, E., Sobol, M., Philimonenko, V. V., Dzijak, R., Venit, T., & Hozák, P. (2013). Involvement of phosphatidylinositol 4,5-bisphosphate in RNA polymerase I transcription. *Journal of Cell Science*, *126*(12), 2730-2739. https://doi.org/10.1242/jcs.123661

Yoo, J. Y., Wang, X. W., Rishi, A. K., Lessor, T., Xia, X. M., Gustafson, T. A., & Hamburger, A. W. (2000). Interaction of the PA2G4 (EBP1) protein with ErbB-3 and regulation of this binding by heregulin. *The British Journal of Cancer*, *82*(3), 683-690. https://doi.org/http://dx.doi.org/10.1054/bjoc.1999.0981

Zhang, Y., Fondell, J. D., Wang, Q., Xia, X., Cheng, A., Lu, M. L., & Hamburger, A. W. (2002). Repression of androgen receptor mediated transcription by the ErbB-3 binding

protein, Ebp1. *Oncogene*, *21*(36), 5609-5618. https://doi.org/http://dx.doi.org/10.1038/sj.onc.1205638